A synoptic- and remote sensing-based analysis of a severe dust storm event over Central Asia

Parya Broomandi [1, 12, #], Kaveh Mohammadpour [2, 3, #], Dimitris G. Kaskaoutis [4], Aram Fathian[5,6,7], Sabur F. Abdullaev[8], Vladimir A. Maslov[8], Amirhossein Nikfal[9], Ali Jahanbakhshi[10], Bakhyt Aubakirova[1], Jong Ryeol Kim [1]*, Alfrendo Satyanaga [1], Alireza Rashki[11], Nick Middleton[13]

[1] *Department of Civil and Environmental Engineering, School of Engineering and Digital Sciences, Nazarbayev University, Kabanbay Batyr Ave. 53, Nur-Sultan 010000 Kazakhstan.*

[2] *Department of Climatology, Faculty of Geographical Sciences, Kharazmi University, Tehran, Iran.*

[3] *Climate Change Technology Transfer to Developing Countries Group (SSPT-PVS), Department of Sustainability, Italian National Agency for New Technologies Energy and Sustainable Development, ENEA, C. R. Casaccia, 00123 Rome, Italy.*

[4] *Institute for Environmental Research and Sustainable Development, National Observatory of Athens, Palaia Penteli, 15236 Athens, Greece.*

[5]UNESCO Chair on Coastal Geo-Hazard Analysis, Research Institute for Earth Sciences, Tehran, Iran.

[6]*Neotectonics and Natural Hazards Institute, RWTH Aachen University, Aachen, Germany.*

[7]*Water, Sediment, Hazards, and Earth-surface Dynamics (waterSHED) Lab, Department of Geoscience, University of Calgary, Canada*

[8]*Academy of Sciences of Republic of Tajikistan, Physical-Technical Institute, Department of Physical Atmosphere, Ayni Str.299/1, 734063, Dushanbe, Tajikistan.*

[9]*Atmospheric Science and Meteorological Research Centre (ASMRC), Tehran, Iran.*

[10] *School of Architecture, Building and Civil Engineering, Loughborough University, Loughborough, UK.*

[11]*Department of desert and arid zones management, Ferdowsi University of Mashhad, Mashhad, Iran*

[12]*Department of Chemical Engineering, Masjed-Soleiman Branch, Islamic Azad University, Masjed-Soleiman, Iran.*

[13]*St Anne's College, University of Oxford, Oxford OX2 6HS, United Kingdom.*

As the first authors with the same authorship contribution

* Corresponding author: Phone: +7 7172 70 9136; Fax: +7 7172 70 9136
Email: jong.kim@nu.edu.kz

Abstract

A severe dust storm blanketing Central Asia on 3-4 November 2021 was investigated employing satellite remote-sensing, synoptic meteorological observations, reanalysis and HYSPLIT back-trajectories. The prevailing meteorological conditions showed an intensification of air subsidence over eastern Kazakhstan, featured in a typical omega-blocking system over the region and two troughs to its west and east axis, one day before the dust storm. The prevailing high-pressure system and temperature gradients over Kazakhstan modulated the dominant anticyclonic wind pattern generated from the south Balkhash basin toward the Caspian Sea, causing a huge dust storm that covered the southern half of Kazakhstan and large parts of Uzbekistan, Tajikistan and Turkmenistan. The dust storm originated in the steppes of southern Kazakhstan by violent downdraft winds. Initially it swept over eastern parts and then the whole of Uzbekistan, reaching the Caspian Sea in the west. Meteorological measurements and HYSPLIT back-trajectories at selected sites in Central Asia (Turkmenabat, Khujand and Tashkent) showed a remarkable dust impact that reduced temperature (by 2-4 °C) and visibility to below 1 km at different periods, as the thick dust plume expanded in various directions. The extremely high PM concentrations (PM_{10}> 10,000 μg m^{-3} in Tashkent) could endanger both human health and the environment, especially in a region suffering from high susceptibility to wind erosion and significant land degradation and desertification. Effective and immediate stabilising measures to control wind erosion in vulnerable areas of Central Asia are warranted.

Keywords: Atmospheric circulation; Dust storms; HYSPLIT; Backward trajectory; Tashkent.

1 Introduction

The ambient air pollution induced by dust storms is associated with a wide range of human health disorders (Middleton, 2020) including (i) respiratory diseases such as bronchial asthma and chronic bronchitis (Al-Hemoud et al., 2018; Kang et al., 2012; Wang et al., 2014), (ii) cardiovascular diseases (Aghababaeian et al., 2021; Aili and Kim Oanh, 2015), (iii) psychological and cognitive disorders (Ghaisas et al., 2016; Gordeev et al., 2013) and (iv) neurodegenerative diseases (Aleya and Uddin, 2020; Chin-Chan et al., 2015; Galán-Madruga et al., 2020; Galán-Madruga and García-Cambero, 2022; Shafiee et al., 2021). Moreover, increased total non-accidental deaths in both adults and children are reported among exposed individuals in areas highly impacted by dust storms (Achilleos et al., 2019; Díaz et al., 2017; Galán-Madruga et al., 2022; Kashima et al., 2016; Perez et al., 2008). High ambient concentrations of dust particles caused by intense dust storms also lead to horizontal visibility reduction, which can have socio-economic impacts in several sectors, including aviation, transport, education, leisure construction and energy production (Middleton et al., 2021; Middleton, 2017; Middleton and Kang, 2017). Dust aerosols, originating from desert areas all over the world, can play an important role in altering Earth's solar radiation balance and the primary productivity of oceans through iron fertilization (Cherian and Quaas, 2020; Jickells et al., 2005; Kok et al, 2018; Schepanski, 2018; Valenzuela et al., 2017). Dust is a major type of tropospheric aerosol and the most common wind-induced climatic phenomenon in the hyperarid, arid and semi-arid regions of Central Asia (CA), accounting for ~25% of total global dust emissions, with significant impacts on regional climate, biogeochemical cycles, loess formation and the hydrological cycle (Booth et al., 2012; Ginoux et al., 2004; Li et al., 2021; Issanova and Abuduwaili, 2017; Uno et al., 2009).

In recent times, dust generation and, consequently, population exposure in CA have escalated due to climate variability and land cover changes, as a result of rapid development, deforestation, enhanced aridity, mining and agricultural activities (Gao and Washington, 2009; Sternberg and Edwards, 2017; UN, 2010; Wiggs et al., 2003). Across CA, the most wind erosive areas and hotspots of dust storm activity are in Kazakhstan (areas surrounding the desiccated Aral Sea, known as the Aralkum Desert, Saryesik Atyrau Desert to the south of Lake Balkhash and Muyunkum Desert to its western end), Turkmenistan (Karakum Desert), Uzbekistan (Kyzylkum Desert), west of Mongolia and northwest China (Tarim Basin, Taklimakan and Gurbantunggut Deserts) (Gholami et al., 2021; Laurent et al., 2006; Song et al., 2021). Beyond climate change (decrease of precipitation and desertification over CA), human intervention, specifically the extended cultivation ploughing up of pastures during the Virgin Lands Programme of the 1950s, have played an important role in the increased wind erosion activity (Goudie and Middleton, 2006; Indoitu et al., 2012; Li and Sokolik, 2018). For example, in Kazakhstan, different degrees of land degradation and desertification occur due to anthropogenic activities, unsustainable land practices such as agricultural activities, and nonrational use of natural sources such as water (Almaganbetov and Grigoruk, 2008; ARLCURK, 2006; Lau et al., 2020; Madruga et al., 2019). Land degradation and desertification are mainly observed in regions under unfavourable ecological conditions such as Lake Balkhash, Caspian lowland and around the dried bed of the Aral Sea (GEF, 2003; NPRK, 2005). The areas in Kazakhstan most vulnerable to wind erosion are the western and southern parts, where the total wind-eroded lands are estimated at about 12.4 and 13.1 million hectares respectively (out of 273.5 million hectares of the Kazakhstan territory). In addition, wind eroded agricultural lands in the eastern and northern parts of the country occupy about 1.28 and 3.87 million hectares respectively, which are subject to accelerated desertification, including around 66% of Kazakhstan's total area (Almaganbetov and Grigoruk, 2008; CSD, 2002). These conditions may lead to changes in regional terrestrial (desertification, wetness of topsoil, surface water resources, surface roughness) and climatic factors (wind and rainfall regimes), facilitating generation of dust storms over CA (Huang et al., 2016, 2017; Mahmoodirad et al., 2016;Wang et al., 2017; Xi and Sokolik, 2015).

Seasonal and inter-annual changes in atmospheric circulation patterns, along with changes in local topography, land use land cover (LULC) and long-term modulations of the climate system, control the dust activity over CA (Kaskaoutis et al., 2017; Nobakht et al., 2021; Shi et al., 2019; 2021; Zhang et al., 2020). Dust particles rising from Central Asia are held responsible for air-quality deterioration over Korea, Japan and Taiwan (Hashizume et al., 2010; Hasunuma et al., 2019), as well as northeast Iran-Afghanistan and other parts of southwest Asia (Kaskaoutis et al., 2016; Mohammadpour et al., 2022). Specific synoptic weather patterns may also favour dust from CA to be transported to the west, impacting Georgia, Belarus and Lithuania (Hongisto and Sofiev, 2004) or even the Balkans and Italy (Tositti et al., 2022). Furthermore, other studies showed that 3% of Asian dust can reach the western USA (Creamean et al., 2014). Dust-raising activity over CA occurs mostly during spring and summer, depending on area and meteorological conditions (Rupakheti et al., 2020, 2019), while dust-induced radiative forcing during intense dust events in Dushanbe, Tajikistan were estimated at -48 ± 12, -85 ± 24 and 37 ± 15 Wm^{-2} at the top of the atmosphere, surface and within the atmosphere, respectively, with even higher values during extreme dust events (Rupakheti et al., 2021).Although several aspects regarding dust sources, climatology of dust activity and dust impacts have been well documented in CA, as discussed above, case studies of severe and long-range transported dust events from this region are rare in the literature (Tositti et al., 2022).

This work analyses a severe dust storm event over CA that affected a large area in southern Kazakhstan, Uzbekistan and Tajikistan on 3–4 November 2021 (Eurasianet, 2021; MKWEATHER, 2021) (**Fig. 1**). A massive dust storm covered Tashkent, the capital of Uzbekistan, where the horizontal visibility decreased to 200 meters and the PM_{10} concentrations spiked at 18,000 µg m^{-3} on 4 November 2021, 30 times above the Uzbekistan maximum acceptable level. Local authorities reported that it was the most extreme sand/dust storm during the last 150 years of monitoring in Tashkent (Uzhydromet, 2021). The true colour imagery of Terra-MODIS sensor, accessible from NASA Worldview (https://worldview.earthdata.nasa.gov) on 4th November 2021, showed a thick dust plume covering parts of south-eastern Kazakhstan, Uzbekistan and north Tajikistan around the Fergana valley (**Fig. 1**). People in Tashkent were advised to stay indoors, avoiding walks and physical activities. On 4th November 2021, the ambulance service received 687 calls from inhabitants in Tashkent seeking help for respiratory problems. Besides hospital admissions, local authorities reported car accidents and casualties due to low horizontal visibility (Uzhydromet, 2021). Moreover, on 5th November, the dust haze caused interruptions in drinking water supply in some districts of Tashkent due to the malfunction in the high-voltage power supply network (Eurasianet, 2021). Dust intrusion also caused a power outage in about 50 villages in the Turkestan region, southeast Kazakhstan, while drivers were stuck on the highway in traffic jams on 4th November 2021, due to reduced visibility (Eurasianet, 2021). Overall, this severe dust storm caused many socio-economic and health impacts for local inhabitants, beyond deterioration of air quality.

This unprecedented dust event in CA undoubtedly needs further investigation of the meteorological conditions and driving mechanisms that initiated such a dust storm. This study investigates the synoptic meteorology and atmospheric circulation patterns that triggered this dust storm event and aims to detect the dust source and the expansion of the dust plumes via SEVIRI satellite imagery. Furthermore, it examines the impact of the dust storm on local meteorological conditions and visibility at specific sites in CA, and provides discussions about land degradation and increased dust activity over CA during the last decades.

2 Methods

2.1 Study region

The Central Asian plains stretch from the shores of the Caspian Sea in the west to the foothills of Altai, Tian-Shan and Pamir Mountains in the east (**Fig. 2**). The Central Asian drylands cover an area of 1.890 million km^2 and are home to about 40 million inhabitants (Indoitu et al., 2012). The area consists of various litho-edaphic desert types such as gravel-gypseous and gravel, sandy, sandy-pebble and pebble, loess, loamy, solonchakous and clayey deserts (Issanova and Abuduwaili, 2017; Gholami et al., 2021; Li et al., 2021). Based on different synoptic processes and meteorological conditions, CA is divided into two climatic zones of northern and southern (Issanova et al., 2015). The northern part has a dry and cold continental Central Asian climate, while the southern region is characterized by a dry and hot climate. In the northern part, the mean annual temperature varies between 5 and 11 °C, while it increases to 13–16.6 °C in the southern part. The annual precipitation over the whole region varies between 80 mm and 200 mm and it is below 100 mm in the desert regions of western

Balkash shore, Kyzylkum, Karakum Deserts and Betpak-Dala (Indoitu et al., 2012; Issanova and Abuduwaili, 2017).

2.2 Ground-based observations

In this study, ground-based hourly data of horizontal visibility, wind speed and temperature at selected stations in Central Asia (i.e., Tashkent, Uzbekistan; Khujand, Tajikistan; Turkmenabat, Turkmenistan) were obtained from the Iowa Environmental Mesonet (https://mesonet.agron.iastate.edu/ASOS/). Additionally, hourly $PM_{2.5}$ data were obtained from the monitoring station in the United States Embassy in Tashkent, Uzbekistan (https://www.airnow.gov/international/us-embassies-and-consulates/).

2.3 Reanalysis data

ERA-5 reanalysis (Hersbach et al., 2020) is produced by European Centre for Medium-Range Weather Forecasts (ECMWF) within the Copernicus Climate Change Service (C3S), which includes a detailed record of the global atmosphere and land surface from 1950 onwards (Hersbach et al., 2020). In this study, ERA-5 reanalysis data was used to obtain meteorological variables of (i) vertical velocity at 300 hPa, (ii) zonal wind at 250 hPa, (iii) geopotential heights at 500 and 850 hPa, (iv) air temperature at 2 m, (v) Mean Sea Level Pressure (MSLP) and (vi) surface vector winds, for the characterization of the daily synoptic conditions at $0.5^{o} \times 0.5^{o}$ spatial resolution over CA during the dust storm event.

The Modern-Era Retrospective Analysis for Research and Applications, version 2 (MERRA-2), is a long-term global reanalysis product with a horizontal resolution of $0.5^{\circ} \times 0.625^{\circ}$ (latitude, longitude) and a temporal resolution varying from hour to month (Galán-Madruga, 2022; Gelaro et al., 2017; Sayer et al., 2019; Shafiee et al., 2019). In this study, the dust loading/dust column mass density (g m^{-2}) was taken over CA on a daily basis around the dust storm event, as MERRA-2 has been proved as an accurate database for studying dust aerosols (Shaheen et al., 2020; Shi et al., 2019).

2.4 Satellite remote sensing observations/products

Visible/IR images of SEVIRI (Spinning Enhanced Visible and Infrared Imager) were employed to monitor the transport of the dust storm in high temporal resolution (~15 mins) (Schepanski et al., 2007, 2009). The infrared channel data from SEVIRI is based on RGB (red-green-blue) image compositions, and dusty pixels in pink or magenta colours are used to monitor the evolution of dust events during both day and night over desert areas (Martínez et al., 2009; Kaskaoutis et al., 2019a).

2.5 HYSPLIT Model

The HYSPLIT-4 (Hybrid Single-Particle Lagrangian Integrated Trajectory) model is widely used for analysis of the air-mass trajectories, dispersion and deposition of aerosols using the Global Forecast System (GFS) meteorological parameters as the initial background field (Ashrafi et al., 2014; Draxler and Hess, 1997). In this study, HYSPLIT air-mass back-trajectories were used at certain receptor sites in Central Asia like Tashkent (41.3° N, 69.26° E), Khujand (40.28° N, 69.63° E) and Turkmenabat (39.03° N, 63.56° E) on the dust storm day (4 November 2021), in order to investigate the dust source and the pathways of the expanded dust plumes that affected several regions in Central Asia (Rashki et al., 2015).

3 Results and discussion

3.1 Satellite remote sensing observations

SEVIRI Visible/IR imagery enables detection of slight or thick dust plumes, as well as subtle variations from one image to another, on high temporal resolution (Schepanski et al., 2009; Alizadeh et al., 2014). In this study, SEVIRI imagery was deployed to monitor the evolution of the dust storm, aiming to identify the source origin, expansion of the dust plume and the affected areas in CA on 4th November 2021 (**Fig. 3**). Strong north-easterlies, which will be analysed in the next section, triggered dust-raising in Zhambyl region, and activated dust sources in Moiynkum, Kyzylorda and eastern Kyzylkum Deserts in the early morning of 4th November 2021 (04:00 UTC). The thick dust plume, shown in bold pink and magenta colours, reached Turkmenabat, Tashkent and Khujand at around 09:00 UTC, 11:00 UTC and 12:00 UTC, respectively. Terra-MODIS true-colour observations and SEVIRI RGB images corroborate detection of a very thick dust plume. However, the intensity of the pink/magenta colours associated with dust in RGB imagery does not absolutely agree with the dust intensity, since the RGB signal could be affected by dust mineralogy, low-temperature inversions and dust-layer height (Brindley et al., 2012; Solomos et al., 2018). The extensive cloudiness over the mountainous ranges is detected in ochre and brown colors in RGB imagery. Note also the change in the desert-surface reflectance colour from light cyan during the early morning hours to yellow, light orange during noon and early afternoon hours on 4 November (**Fig. 3**).

3.2 Atmospheric dynamics during the dust storm

This section analyses the atmospheric circulation patterns in the upper, middle, and lower troposphere during a 6-day period (1–6 November 2021) around the dust storm day (4 November 2021), aiming to reveal the dynamic conditions that were associated with the genesis, expansion and dissipation of the dust storm (**Figs. 4-7**). Prior to the dust storm, on 1st November, a typical cold atmospheric circulation formed over eastern Europe and the Balkan Peninsula, detected by a deep trough, which started to dissipate on 3rd November (**Fig. 4a-c**). In the upper troposphere, these conditions were characterized by two relatively weak polar and subtropical jet streams over Russia and south Asia, respectively. The polar jet stream was progressively moving from central-west Siberia to east Kazakhstan, while marginal changes were observed in the sub-tropical jet stream, with a core of above 45 ms^{-1} over the Ganges valley and the

Himalayas (**Fig. 5a-c**). The dynamic conditions created subsidence behind the subtropical jet core over the east of Iran, Afghanistan and Pakistan, while negative omega values at 300 hPa dominated over the Kazakhstan-Russia border, associated with the polar jet (**Fig. 5a-c**). In the meanwhile, the cold Siberian anticyclone was dominant over eastern Siberia, creating a strong gradient of geopotential heights across the Russia-Kazakhstan border. A high-pressure ridge prevailed on days prior to dust storm stretching from the Middle East and Iran to the Caspian Sea and western Russia, carrying warmer air masses over the region. These conditions created an omega blocking system over CA and Russia on days prior to the dust storm, while the axis of this ridge progressively shifted from southeast-to-northwest (1st November) to southwest-northeast on 4th November (**Fig. 4**), thus changing the upper-troposphere circulation. The upper-level conditions accompanied by stretching a trough in mid troposphere (500 hPa) over the northern borders of Kazakhstan, increased the instability along troposphere, which was induced to penetrate cold air masses from the Siberian region into CA. On 3rd November, just prior to the dust storm, the polar jet, with a core of 35-45 ms^{-1}, moved from south Russia to east Kazakhstan, causing negative omega at 300 hPa over the region (**Fig. 5a-c**). These conditions maximized air subsidence over the Kazakhstan-Russia border, which was accompanied by the eastward replacement of the polar jet with air upward motion over southeast Kazakhstan (**Fig. 5c**). The circulation at 500 hPa level featured a typical omega blocking pattern, with a large ridge over west Russia and two troughs to its west and east, whereas the latter was much deeper than the former extending into the whole territory of Kazakhstan. A strong surface-temperature gradient was created along north Kazakhstan, with the minimum temperature below −30 °C (Sun et al., 2020), which was moving northwards affecting the central-eastern part of Kazakhstan on 3rd – 4th November, with characteristics of a cold front associated with the Siberian anticyclone. Furthermore, the establishment of the polar jet stream strengthened the vertical instability, helping the convergence and invasion of cold air mass into east Kazakhstan.

The atmospheric circulation on 4th November had a notable difference from that on 3rd November, mostly detected by the strengthening of the jet stream over eastern Kazakhstan (wind speeds above 45 ms^{-1}). This jet stream was expanded over a much lower area, which was affected by an intensified trough, as a tongue of cold-air intrusion from the Siberian anticyclone (**Fig. 4d, 5d**). These meteorological conditions triggered highest negative omega values highlighted an upward air motion in the upper troposphere over east Kazakhstan and surroundings and is likely to be highly associated with the dust storm outbreak, as also shown in previous studies over the Middle East and the Mediterranean (Kaskaoutis et al., 2019b; Rashki et al., 2019; Hamzeh et al., 2021). These dynamic conditions also induced an intense gradient between northern divergence and southern convergence in Central Asia. Furthermore, in the middle troposphere (500 hPa), the south-westward trough became deeper compared to previous day and it is stretched from Siberia to Iran, with the expanded ridge north-eastward, covering central Russia (**Fig. 4d**). The omega blocking system, accompanied with the Siberian anticyclone and favoured by the establishment of the upper-level jet stream over east Kazakhstan, seem to play a major role in the dust storm outbreak in east Kazakhstan. Although the atmospheric circulation patterns during intense dust storms in CA have not been well documented, being also variable depending on season and dust event (Kaskaoutis et al., 2019b; Tositti et al., 2022), the role of the Siberian anticyclone, the position and movement of the upper-level jet stream seem to be very important factors controlling dust activity over CA during the cold period of the year.

On 5th November, the strong zonal winds at 250 hPa (> 25 ms^{-1}) covered an extended area from Italy toward western Russia (**Fig. 5e**), which was further extended to Siberia on the next day, while the upper-level jet over eastern Kazakhstan was dissipated and moved further to the south, practically merged with the subtropical upper-level jet over north India and the Tibetan Plateau (**Fig. 5f**). This weather pattern reflects rather stable upper-troposphere conditions accompanied by descending air, with positive omega values, over nearly the whole CA. The negative omega values prevailed in the northern edge of the subtropical jet (**Fig. 5e**), became more active air ascending over the trough-affected areas contributing to suction of cold air masses toward Tajikistan and northeast Pakistan on 5th November, when an expanded trough tongue covered the southeast Central Asian countries, extended over Iran (**Fig. 4e**). The omega blocking system over CA was significantly dissipated after the dust storm day and was limited to southern latitudes, as a ridge over the East Mediterranean - Middle East (EMME) region. These conditions limited invasion of polar cold air and transferred warmer air masses over CA and pushed the trough toward the east, while a zonal circulation was established at northern latitudes over Russia (**Fig. 4e, f**).

The relative positions and intensity of the low- and high-pressure systems accompanied by the polar and subtropical jet streams at upper-levels, generally control the intensity of the surface regional winds and dust outbreaks (Francis et al., 2018, 2022; Mohammadpour et al., 2021b; 2022a, b). The meteorological conditions due to Caspian's ridge at 500 hPa level facilitated the formation of high-pressure conditions at lower troposphere and at the surface over CA countries (**Fig. 6**). These conditions seem to modulate the dust activity over the region (Kaskaoutis et al., 2016; Shi et al., 2019). The dynamic pressure pattern on 2nd November, which was a combination of two weak high-pressure systems over north Russia and CA on previous day, was characteristic of the omega blocking at the lower troposphere (850 hPa) and at the surface, with high-pressure conditions over central Siberia. The geopotential heights at 850 hPa presented even higher values on the next days (3rd and 4th November 2021), with closed high-pressure systems over Kazakhstan, while at surface, high-pressure conditions of above 1040 hPa dominated over the whole Kazakhstan territory. The synoptic meteorology over the examined domain clearly dominated by this high-pressure system over CA, while lower pressure conditions prevailed in south Asia, the EMME region and in central/western Europe **(Fig. 6a-d**). This intense and expanded high-pressure system over CA (>1600 gpm; >1040 hPa over Kazakhstan), was a triggering dynamic for the formation of dust storm on 4 November 2021, while on the days after the dust storm, the core of the high-pressure system at 850 hPa was expanded over a larger area, slightly moved towards the east, and then significantly dissipated (**Fig. 6e-f**). These meteorological conditions were different from those usually prevailed during dust storms over southwestern CA in spring and summer that were attributed to high-pressure system over the Caspian Sea and thermal low-pressure over topographic-low areas in southern latitudes (Cheng et al., 2019; Li et al., 2019; Mohammadpour et al., 2021b, 2021a). Overall, MSLP dynamics highly controlled the wind regime on days prior, during and after the intense dust storm of 4th November 2021 over southeastern Kazakhstan.

Figure 6 shows the vector wind at the surface along with the spatial distribution of dust loading (in g m^{-2}) obtained from MERRA-2 over Central Asia from 1 to 6 November 2021. The establishment of the high-pressure system over the northern part of CA on 2nd November, modified the wind regime from the previous day, with a strong anticyclonic flow over Kazakhstan, which further intensified on 3rd November. The easterly winds, propagated from the southern flanks of the high-pressure system over the southern part of CA, passed over Moiynkum, eastern Kyzylkum, Aralkum and Karakum Deserts (Zhou et al., 2019) and advected high dust loading covering a wide area till the shores of the Caspian Sea (**Fig. 7b-c**). At the same time, winter Shamal wind facilitated increased dust loading over the Syrian–Iraqi plains. A strong northerly/north-easterly flow dominated over the dust-source area, as well as over the alluvial dried beds in the Balkhash basin in east Kazakhstan, favouring dust emissions. On the dust storm day (4 November 2021), the associated changes in the distribution of G850, MSLP and wind regimes over the central Asian countries, indicated that the strengthened high-pressure system intensified the dominant anticyclonic wind pattern compared to previous days. The prevailing surface wind propagated from the southern Balkhash basin blowing toward the Caspian Sea and affected the southern half of Kazakhstan and nearly whole territories of Uzbekistan and Turkmenistan (**Fig. 7d**). These areas are covered by high columnar dust loading greater than 1.1 g m^{-2}, probably emitted from the various deserts such as Aralkum, Kyzylkum, Trans-Unguz, and central Karakum and alluvial dried beds of the Caspian lowlands (Nobakht et al., 2021). Therefore, apart from the thick dust plume that covered the Tashkent area on 4 November 2021 and caused several socio-economic and health impacts on local population, the north-easterly/easterly flows generated from the centre of the anticyclone over Kazakhstan facilitated an extensive dust blanket over the southern parts of CA, also covering the Caspian Sea (**Figs. 7d**). The synoptic conditions on 5^{th} November presented large similarities with the dust storm day, and this is also shown in the vector wind pattern, while the dust loading was progressively dissipated with lower values (~0.5 to 0.7 g m^{-2}) over southern CA (**Fig. 7e**). MERRA-2 observations show high dust loading over the Tarim Basin and Taklimakan Desert, likely caused by convergence of winds over these desert areas and a significant dust transport from Libya towards south Italy and the Balkans due to strong southerlies. On the next day, 6^{th} November 2021 (**Fig. 7f**), the dust loading over Central Asia was further reduced, while the dust hotspots over Taklimakan, central Mediterranean and the Indo-Gangetic plains intensified.

3.3 Ground-based meteorological observations

3.3.1 $PM_{2.5}$ concentrations in Tashkent

Figure 8 shows the variation of hourly $PM_{2.5}$ concentrations from the air quality station located in the US embassy in Tashkent, Uzbekistan from 1 to 10 November 2021. The $PM_{2.5}$ concentrations are color-coded with the Air Quality Index (AQI) data classified for the six AQI categories (good, satisfactory, moderate, poor, very poor and severe) related to various health clusters for the local population (from good to hazardous). Around 18:00 pm on 4 November 2021, there was a spike in $PM_{2.5}$ levels caused by the arrival of the severe dust storm originated from southeast Kazakhstan. $PM_{2.5}$ concentrations raised above 900 µg m^{-3} during the afternoon hours on 5th November. On 5 and 6 November, the AQI values were categorized in the very unhealthy and hazardous class for any group of population in Tashkent. There was a gap in $PM_{2.5}$ recordings between 22:00 pm on 4th November and 17:00 pm on 5th November, probably attributable to instrument failure caused by the severe PM concentrations. The daily mean $PM_{2.5}$ concentrations were 393 µg m^{-3} (26 times higher than the guideline level of 15 µg m^{-3} according to WHO), 215 µg m^{-3} (14 times higher) and 111 µg m^{-3} (7.5 times higher), on 6th, 7th and 8th November, respectively (WHO, 2021). The intense dust haze (caused by particles raised into the atmosphere by a recent dust or sand storm) started dissipating in the evening hours of 6th November. Still, dust particles remained till about 15th November when heavy rain helped to wet deposition of PM. Similarly elevated $PM_{2.5}$ concentrations during severe dust storms have been reported in other parts of the world (Dumka et al., 2019; Hussein et al., 2020; Wu et al., 2021). In Beijing, China, Wu et al. (2021) reported daily mean $PM_{2.5}$ concentrations exceeding 200 µg m^{-3} on 15th March 2021 caused by an intense dust storm originating in Mongolia. In addition, $PM_{2.5}$ levels were ~109 µg m^{-3} on 25th July 2018 in Amman, Jordan during a dust storm episode originating in the Sahara Desert (Hussein et al., 2020; Shafiee et al., 2017).

3.3.2 Changes in horizontal visibility and 10-m wind speed

Figure 9 shows the hourly ground-based measurements of horizontal visibility and wind speed during 1-6 November 2021 at three sites in CA (Turkmenabat, Tashkent and Khujand) directly affected by the dust storm. In Turkmenabat, the dust arrived at around 09:00 UTC on 4th November and lasted for approximately 15 hours. During the arrival of the dust storm, visibility dropped drastically from about 10 km to 1 km, accompanied by a notable increase of wind speed from about 4 ms^{-1} to 10–12 ms^{-1} during the peak of the dust storm over the site (Fig. 8a). The minimum horizontal visibility was recorded at 15:00 UTC with a value of 692 m, when the wind speed was 12.5 ms^{-1}.

In Tashkent, horizontal visibility varied considerably on days prior to the dust storm, while the large gaps in visibility were accompanied by weak-to-calm winds (< 1–2 ms^{-1}) that favoured the accumulation of anthropogenic aerosols and pollutants near the ground. This is a characteristic atmospheric condition in urban-polluted environments, where the weak winds and temperature inversions are responsible for trapping aerosols near the ground, which contribute to scattering of solar radiation and visibility degradation (Dumka et al., 2017; Liakakou et al., 2020). However, on 4 November the dramatic decrease in visibility was accompanied by a notable increase in wind speed (6–7 ms^{-1}) signalling the arrival of the dust storm (**Fig. 9b**). As mentioned above, Tashkent was severely affected by this severe dust storm, which reduced visibility below 1000 m at 15:00 UTC and below 200 m between 16:00–18:00 UTC (4 November 2021). Dust aerosols over the city remained for the next 8 days, contributing to the reduced visibility (< 2–3 km; **Fig. 9b**) and the increased $PM_{2.5}$ concentrations compared to pre dust storm days.

In Khujand, the dust plume arrived at 12:00 UTC and immediately caused a reduction in visibility to below 2.5 km. As the dust plume thickened, visibility dropped below 1 km for about 7 hours. At the time of dust arrival, the wind speed in Khujand was 10 ms^{-1}, while the changes in wind speed and visibility due to arrival of the dust storm were mostly similar in all the examined stations. This indicated that the thick dust plume that blanketed these sites was approaching in the form of a dust wall accompanied by strong near-surface winds, resulting in a strong negative correlation between wind speed and horizontal visibility. On the days prior to the dust storm, visibility records were mostly affected by local activities in the cities, while on the days after the dust storm, the visibility remained at general low levels, until atmospheric cleaning.

3.3.3 Variations in surface air-temperature

Figure 10 shows the temperature variation during the first half of November 2021 in Tashkent, Khujand, and Turkmenabat. The data showed that the dust intrusion on 4 November significantly changed the temperature regime in the region. As mentioned above, dust particles remained in the atmosphere for a long time, until heavy rain cleaned the air on 15th November 2021 in Tashkent and Khujand. In Turkmenabat, there was no rain, but horizontal visibility started to increase above 10 km from 14th November 2021, after the removal of dust aerosols.

In Turkmenabat, the daytime air temperature decreased on 4th November 2021 compared to 3rd November 2021 (before dust event) and 11th November 2021 (after dust event) by -11.8°C and -3.4°C , respectively. However, opposite changes in nighttime temperature occurred by +5.1°C and +10.4°C relative to the days before and after the dust event. A similar situation was observed in Tashkent, where the daytime temperature decreased by -9.8°C and -10.1°C relative to 2nd November 2021 and 12th November 2021, while at night there was an increase in temperature by +2.3°C and +2.9°C , respectively. In Khujand, the dust storm on 4th November 2021, caused a notable decrease in daytime air temperature by -8.6°C and -12.5°C with respect to 2nd and 13th November 2021. The respective nighttime air temperatures were higher on 4th November by +9.5°C and +8.4°C compared to aforementioned days. It should be noted that apart from the aforementioned temperature amplitudes between the dust day and specific days before and after the dust event, the arrival of the dust storm over each station caused a notable decrease in air temperature (**Fig. 10**), which is partly attributed to presence of a cold front associated with dust and to radiative impact of dust on solar radiation.

Similar temperature changes with the arrival of intense dust storms have been reported at several sites worldwide (Alharbi et al., 2013; Kaskaoutis et al., 2019b; Maghrabi et al., 2011; Prakash et al., 2015). Kaskaoutis et al. (2019b) reported a considerable decrease in maximum temperature (~8–11°C) due to dust radiative cooling and the passage of a cold front on 5th -6th February 2019 compared to 4th February 2019 in Zabol, Iran. The Middle East also experienced a remarkable reduction of −6.7 °C in temperature due to the dust radiative cooling during severe dust storms from 18th to 22nd March 2012 (Prakash et al., 2015). According to previous studies, mineral dust particles have an important role in global energy balance via both direct (on solar radiation) and indirect (on clouds) effects (Kok et al., 2018, 2017). Generally, when shortwave radiation encounters dust aerosols, cooling happens because some radiation does not reach the Earth's surface. On the other hand, dust particles can also absorb longwave radiation, emitted by the earth, atmosphere and clouds, and contributes to planetary warming (Kok et al., 2018; Mahowald et al., 2014; Miller et al., 2006; Tegen and Lacis, 1996).

3.4 Backward trajectory analysis

To monitor the movement of the dust storm that affected the three receptor sites, the HYSPLIT-4 model was implemented to analyse the transport pathway of dust particles through 3-hour time intervals up to 48 hours before dust episodes reaching the study locations (**Fig. 11**). The starting point of trajectories was in Turkmenabat on 4/11/2021 at 09:00 UTC, in Tashkent on 4/11/2021 at 11:00 UTC, and in Khujand on 4/11/2021 at 12:00 UTC. The arriving height of the air masses at the receptor sites was set at mid boundary layer height to guarantee both transition and ending of dust trajectories in the boundary layer (Broomandi et al., 2021; Karaca et al., 2009).

Turkmenabat, in central Turkmenistan, was hit by the dust plume on 4th November at 09:00 UTC, while the air masses at the altitude of 275 m originated from north/north-eastern directions, i.e., Qaraghandy and Pavlodar in Kazakhstan (**Fig. 11a**), passing over southeast

Kazakhstan, where the dust storm was generated (**Fig. 2b**). Similar air mass pathways are observed in Tashkent (**Fig. 11b**), which was upwind of the dusty air masses that hit Turkmenabat. The starting points of the majority of the air masses at 130 m altitude (mid-boundary layer height) were from eastern and central Kazakhstan, and continued to the Almaty region, Jambyl and south Kazakhstan, before reaching Tashkent (**Fig. 11b**). The dusty air masses that hit Khujand travelled over the same regions (**Fig. 11c**), while the results of trajectories simulation were consistent with the SEVIRI Visible/IR imagery (**Fig. 3**) during the dust intrusion, indicating that air masses were mainly originated from south-western parts of Russia, as well as eastern, central, and southern Kazakhstan. While they were passing over dust sources located in south Kazakhstan, including Kyzylorda and Kyzylkum Deserts, the transport of dust particles was facilitated by the northeast winds toward Turkmenabat, Khujand and Tashkent in the afternoon of 4^{th} November 2021.

3.5 Land degradation in Central Asia and future projections

The 4^{th} November severe dust storm over south-eastern Kazakhstan that affected a large area in CA, was a unique and rare phenomenon, in terms of its intensity, that happened in an area vulnerable to dust emissions and with continuous soil degradation during recent decades due to ongoing human interventions (Aiman et al., 2018; Baubekova et al., 2021; Guney et al., 2020; Kismelyeva et al., 2021; Ramazanova et al., 2021). Apart from the high PM concentrations during dust storms, potentially toxic elements (PTEs) as soil contaminants transported by dust may add more health and ecological concerns over the CA region.

Due to the potentially toxic-contaminated soils in arid areas of CA, it is recommended to perform site-specific studies, also examining the chemical composition during intense dust storms. It is also highly recommended to take effective and immediate stabilising measures to control the wind erosion in vulnerable areas. Since sand and dust storm (SDS) activity is an alarming challenge to sustainable development in more than 150 countries that are directly affected by SDS worldwide (Middleton and Kang, 2017), it is necessary to prepare suitable climate adaptation and mitigation strategies, developing more reliable and accurate early warning systems and quantifying the impacts to societal implications in both national and regional scales. A transboundary multi-hazard risk assessment is also essential in analysing the cause-and-effect relationships and helping policymakers to fully understand the required dynamics and complexity of policy actions. Such transboundary dialogue and collaboration between the affected countries lead to policy interventions reflecting the geospatial link among the origins and receptors, which can positively influence both adaption and mitigation aspects.

4 Conclusions

This study investigated a severe dust storm that occurred on 4th November 2021 over Central Asia, a phenomenon unprecedented in this region over the last 150 years (Eurasianet, 2021) that caused an increase of PM_{10} concentrations above 18,000 μg m^{-3} in Tashkent, Uzbekistan. Meteorological measurements at selected sites in Central Asia including Turkmenabat in Turkmenistan, Khujand in Tajikistan and Tashkent in Uzbekistan showed that a large part of Central Asia was highly impacted by this unique dust storm, which reduced horizontal visibility to 200–1000 m and daytime temperature by 2-4 °C at different time periods. The thick dust plume that blanketed these sites approached in the form of a dust wall accompanied by strong near-surface winds.

Favourable meteorological conditions for the formation of an intense dust storm prevailed both in the upper and lower troposphere over Central Asia and more specifically over the eastern Kazakhstan, which was detected by SEVIRI imagery as the main dust-source region. A high-pressure ridge prevailed during the day prior to the dust storm, stretching from the Middle East and Iran to the Caspian Sea and west Russia, creating a typical omega blocking pattern at 500 hPa level, with a large ridge over west Russia and two troughs to its west and east. The axis of the ridge progressively shifted from southeast-to-northwest (1st November) to southwest-northeast on 4th November, resulting in a strong surface air-temperature gradient and invasion of cold air masses associated with the anticyclonic system over Kazakhstan. The intense high-pressure system over CA was a triggering dynamic force for the formation of the dust storm on 4th November 2021, due to strong easterly winds from the southern flanks of the high-pressure system toward the southern part of CA, passing over Aralkum, Moiynkum, Kyzylorda, eastern Kyzylkum, Trans-Unguz, and central Karakum Deserts. On the dust storm day, an intense jet stream with core wind values of about 4 ms^{-1} was located just above the dust-source region in southeastern Kazakhstan.

HYSPLIT air-mass back trajectories at the receptor sites of Turkmenabat, Khujand, and Tashkent were consistent with SEVIRI satellite data regarding the apportionment of the dust intrusions at each site, indicating that the dusty air masses mainly originated from the south-eastern parts of Kazakhstan, including Kyzylorda and Kyzylkum Deserts. The transport of dust plumes was facilitated by the northeast winds toward Turkmenabat, Khujand, and Tashkent in the afternoon of 4th November 2021. Central Asia is considered a highly sensitive area in view of climate change due to projections of precipitation decrease and increased possibility of prolonged droughts. Under such climatic conditions in the future, severe dust storms in the area will inevitably follow an increasing frequency, causing large deterioration to atmospheric environment and major socio-economic issues in the countries of Central Asia.

Acknowledgments

The authors acknowledge the financial support for the NU projects (Nazarbayev Research Fund SOE2017003 & 11022021CRP1512). Kawe | Kaveh M. acknowledges grant support by Iran National Science Foundation (INSF) under post-doctoral project No. 4001142. A.R acknowledges support by Iran National Science Foundation (INSF) under project No 99003984.

The authors thank Earth data, NASA, the ECMWF and Copernicus teams for providing the MODIS, MERRA-2 and ERA-5 products used in this work.

Conflict of interest

The authors declare that they have no conflict of interest.

Credit Authorship Contribution Statement

Parya Broomandi: Conceptualization, Methodology, Software, Data Curation, Formal Analysis, Validation, Investigation, Visualization, Writing - Original Draft.

Kaveh Mohammadpour: Conceptualization, Methodology, Software, Data Curation, Formal Analysis, Validation, Investigation, Visualization, Writing - Original Draft.

Dimitris G. Kaskaoutis: Conceptualization, Methodology, Validation, Writing - Review & Editing.

Sabur F. Abdullaev: Formal Analysis, Data Curation, Resources.

Vladimir A. Maslov: Formal Analysis, Data Curation, Resources.

Amirhossein Nikfal: Data Curation, Software.

Aram Fathian: Data Curation, Software.

Ali Jahanbakhshi: Data Curation, Software.

Bakhyt Aubakirova: Data Curation

Jong Ryeol Kim: Funding acquisition, Project administration Resources.

Alfrendo Satyanaga: Funding acquisition, Project administration, Resources.

Alireza Rashki: Formal Analysis, Visualization.

Nick Middleton: Original concept, Supervision, Validation, Writing - Review & Editing.

Data availability

Data is available on request from the authors.

Ethical Approval

Not applicable.

Consent to participate

Not applicable.

Consent for publication

Not applicable.

Data availability

Data is available on request from the authors.

Ethical Approval

Not applicable.

Consent to participate

Not applicable.

Consent for publication

Not applicable.

References

Achilleos, S., Al-Ozairi, E., Alahmad, B., Garshick, E., Neophytou, A.M., Bouhamra, W., Yassin, M.F., Koutrakis, P., (2019). Acute effects of air pollution on mortality: A 17-year analysis in Kuwait. *Environ. Int.* 126, 476–483. https://doi.org/10.1016/j.envint.2019.01.072

Aghababaeian, H., Ostadtaghizadeh, A., Ardalan, A., Asgary, A., Akbary, M., Yekaninejad, M.S., Stephens, C., (2021). Global Health Impacts of Dust Storms: A Systematic Review. *Environ. Health Insights* 15, 11786302211018390. https://doi.org/10.1177/11786302211018390

Aili, A., Kim Oanh, N.T., (2015). Effects of dust storm on public health in desert fringe area: Case study of northeast edge of Taklimakan Desert, China. Atmos. *Pollut. Res.* 6, 805–814. https://doi.org/10.5094/APR.2015.089

Aiman, N., Gulnaz, S., Alena, M., (2018). The characteristics of pollution in the big industrial cities of Kazakhstan by the example of Almaty. *J. Environ. Heal. Sci. Eng.* 16, 81–88. https://doi.org/10.1007/s40201-018-0299-1

Aleya, L., Uddin, M.S., (2020). Environmental pollutants and the risk of neurological disorders. *Environ. Sci. Pollut. Res.* 27, 44657–44658. https://doi.org/10.1007/s11356-020-11272-3

Alharbi, B., Maghrabi, A., Tapper, N., (2013). The March 2009 Dust Event in Saudi Arabia: Precursor and Supportive Environment. *Bull. Am. Meteorol. Soc.* 94, 515–528.

https://doi.org/10.1175/BAMS-D-11-00118.1

Al-Hemoud, A., Al-Dousari, A., Al-Shatti, A., Al-Khayat, A., Behbehani, W., Malak, M., (2018). Health Impact Assessment Associated with Exposure to PM10 and Dust Storms in Kuwait. *Atmosphere* (Basel). 9. https://doi.org/10.3390/atmos9010006

Almaganbetov, N., Grigoruk, V., (2008). Degradation of Soil in Kazakhstan: Problems and Challenges BT - Soil Chemical Pollution, Risk Assessment, Remediation and Security, in: Simeonov, L., Sargsyan, V. (Eds.), . Springer Netherlands, Dordrecht, pp. 309–320.

ARLCURK, (2006). Analytical Report on Land Conditions and Use in the Republic of Kazakhstan.

Ashrafi, K., Shafiepour-Motlagh, M., Aslemand, A., Ghader, S., (2014). Dust storm simulation over Iran using HYSPLIT. *J. Environ. Heal. Sci. Eng.* 12, 9. https://doi.org/10.1186/2052-336X-12-9

Baubekova, A., Akindykova, A., Mamirova, A., Dumat, C., Jurjanz, S., (2021). Evaluation of environmental contamination by toxic trace elements in Kazakhstan based on reviews of available scientific data. Environ. *Sci. Pollut. Res.* 28, 43315–43328. https://doi.org/10.1007/s11356-021-14979-z

Booth, B.B.B., Dunstone, N.J., Halloran, P.R., Andrews, T., Bellouin, N., (2012). Aerosols implicated as a prime driver of twentieth-century North Atlantic climate variability. *Nature* 484, 228–232. https://doi.org/10.1038/nature10946

Brindley, H., Knippertz, P., Ryder, C., Ashpole, I., (2012). A critical evaluation of the ability of the Spinning Enhanced Visible and Infrared Imager (SEVIRI) thermal infrared redgreen-blue rendering to identify dust events: theoretical analysis. *J. Geophys. Res.* 117, D07201.

Broomandi, P., Karaca, F., Guney, M., Fathian, A., Geng, X., Kim, J.R., (2021). Destinations frequently impacted by dust storms originating from southwest Iran. *Atmos. Res.* 248, 105264. https://doi.org/10.1016/j.atmosres.2020.105264

Cavazos-Guerra, C., Todd, M.C., (2012). Model Simulations of Complex Dust Emissions over the Sahara during the West African Monsoon Onset. *Adv. Meteorol.* 2012, 351731. https://doi.org/10.1155/2012/351731

Chen, T., Bao, A., Jiapaer, G., Guo, H., Zheng, G., Jiang, L., Chang, C., Tuerhanjiang, L., (2019). Disentangling the relative impacts of climate change and human activities on arid and semiarid grasslands in Central Asia during 1982-2015. *Sci. Total Environ.* 653, 1311–1325. https://doi.org/10.1016/j.scitotenv.2018.11.058

Chin-Chan, M., Navarro-Yepes, J., Quintanilla-Vega, B., (2015). Environmental pollutants as risk factors for neurodegenerative disorders: Alzheimer and Parkinson diseases. *Front. Cell. Neurosci.* 9, 124. https://doi.org/10.3389/fncel.2015.00124

Creamean, J., Spackman, J., Davis, S., White, A., (2014). Climatology of Long-Range Transported Asian Dust along the West Coast of the United States. *J. Geophys. Res. Atmos.* 119. https://doi.org/10.1002/2014JD021694

CSD, (2002). Commission on Sustainable Development, UNDP, Country Profile Report, World Summit on Sustainable Development,. Johannesburg.

Díaz, J., Linares, C., Carmona, R., Russo, A., Ortiz, C., Salvador, P., Trigo, R.M., (2017). Saharan dust intrusions in Spain: Health impacts and associated synoptic conditions. *Environ. Res.* 156, 455–

467. https://doi.org/10.1016/j.envres.2017.03.047

Dumka, U.C., Kaskaoutis, D.G., Francis, D., Chaboureau, J.-P., Rashki, A., Tiwari, S., Singh, S., Liakakou, E., Mihalopoulos, N., (2019). The role of the Intertropical Discontinuity region and the heat-low in dust emission and transport over the Thar desert - India: A pre-monsoon case study. *J. Geophys. Res.* 124, 13197 - 13219, https://doi.org/10.1029/2019JD030836

Dumka, U.C., Tiwari, S., Kaskaoutis, D.G., Hopke, P.K., Singh, J., Srivastava, A.K., Bisht, D.S., Attri, S.D., Tyagi, S., Misra, A., Pasha, G.S.M., (2017). Assessment of PM2.5 chemical compositions in Delhi: primary vs secondary emissions and contribution to light extinction coefficient and visibility degradation. *J. Atmos. Chem.* 74, 423-450.

Eurasianet, 2021. Severe dust storm engulfs Uzbekistan.

Galán-Madruga, D., (2022). Urban air quality changes resulting from the lockdown period due to the COVID-19 pandemic. *Int. J. Environ. Sci. Technol.* https://doi.org/10.1007/s13762-022-04464-6

Galán-Madruga, D., García-Cambero, J.P., (2022). An optimized approach for estimating benzene in ambient air within an air quality monitoring network. *J. Environ. Sci.* 111, 164–174. https://doi.org/10.1016/j.jes.2021.03.005

Galán-Madruga, D., Terroba, J.M., Dos Santos, S.G., Úbeda, R.M., García-Cambero, J.P., (2020). Indoor and Outdoor PM(10)-Bound PAHs in an Urban Environment. Similarity of Mixtures and Source Attribution. *Bull. Environ. Contam. Toxicol.* 105, 951–957. https://doi.org/10.1007/s00128-020-03047-w

Galán-Madruga, D., Ubeda, R.M., Terroba, J.M., Dos Santos, S.G., García-Cambero, J.P., (2022). Influence of the products of biomass combustion processes on air quality and cancer risk assessment in rural environmental (Spain). *Environ. Geochem. Health* 44, 2595–2613. https://doi.org/10.1007/s10653-021-01052-4

Gao, H., Washington, R., (2009). The spatial and temporal characteristics of TOMS AI over the Tarim Basin, China. *Atmos. Environ.* 43, 1106–1115. https://doi.org/10.1016/j.atmosenv.2008.11.013

GEF, 2003. Global Environment Facility, Operating Program on Sustainable Land Management # 15.

Gelaro, R., McCarty, W., Suárez, M.J., Todling, R., Molod, A., Takacs, L., Randles, C.A., Darmenov, A., Bosilovich, M.G., Reichle, R., (2017). The modern-era retrospective analysis for research and applications, version 2 (MERRA-2). *J. Clim.* 30, 5419–5454.

Ghaisas, S., Maher, J., Kanthasamy, A., (2016). Gut microbiome in health and disease: Linking the microbiome-gut-brain axis and environmental factors in the pathogenesis of systemic and neurodegenerative diseases. *Pharmacol. Ther.* 158, 52–62. https://doi.org/10.1016/j.pharmthera.2015.11.012

Gholami, H., Mohamadifar, A., Malakooti, H., Esmaeilpour, Y., Golzari, S., Mohammadi, F., Li, Y., Song, Y., Kaskaoutis, D., Fitzsimmons, K., Collins, A., (2021). Integrated modelling for mapping spatial sources of dust in central Asia - An important dust source in the global atmospheric system. *Atmos. Pollut. Res.* https://doi.org/10.1016/j.apr.2021.101173

Ginoux, P., Prospero, J.M., Torres, O., Chin, M., (2004). Long-term simulation of global dust distribution with the GOCART model: correlation with North Atlantic Oscillation. *Environ. Model. Softw.* 19, 113–128. https://doi.org/10.1016/S1364-8152(03)00114-2

Gordeev, S.A., Posokhov, S.I., Kovrov, G. V, Katenko, S. V, (2013). Psychophysiological characteristics of panic disorder and generalized anxiety disorder. Zhurnal Nevrol. i psikhiatrii Im. S.S. Korsakova 113, 11–14.

Goudie, A., Middleton, N., (2006). Desert Dust in the Global System. *Desert Dust Glob. Syst.* 1–287. https://doi.org/10.1007/3-540-32355-4

Guney, M., Kumisbek, A., Akimzhanova, Z., Kismelyeva, S., Beisova, K., Zhakiyenova, A., Inglezakis, V., Karaca, F., (2021). Environmental Partitioning, Spatial Distribution, and Transport of Atmospheric Mercury (Hg) Originating from a Site of Former Chlor-Alkali Plant. *Atmos.* https://doi.org/10.3390/atmos12020275

Hamzeh, N.H., Karami, S., Kaskaoutis, D.G., Tegen, I., Moradi, M., Opp, Ch., (2021). Atmospheric Dynamics and Numerical Simulations of Six Frontal Dust Storms in the Middle East Region. *Atmosphere* 12, 125. https://doi.org/10.3390/atmos12010125

Hashizume, M., Ueda, K., Nishiwaki, Y., Michikawa, T., Onozuka, D., (2010). Health effects of Asian dust events: a review of the literature]. *Nihon Eiseigaku Zasshi.* 65, 413–421. https://doi.org/10.1265/jjh.65.413

Hasunuma, H., Ichinose, T., Ueda, K., Odajima, H., Kanatani, K., Shimizu, A., Takami, A., Takeuchi, A., Nishiwaki, Y., Watanabe, M., Hashizume, M., (2019). Health Effects of Asian Dust Events: A Literature Review Update of Epidemiological Evidence. *Nihon Eiseigaku Zasshi.* 74. https://doi.org/10.1265/jjh.19010

Hersbach, H., Bell, B., Berrisford, P., Hirahara, S., Horányi, A., Muñoz-Sabater, J., Nicolas, J., Peubey, C., Radu, R., Schepers, D., (2020). The ERA5 global reanalysis. *Q. J. R. Meteorol. Soc.* 146, 1999–2049.

Hongisto, M., Sofiev, M., (2004). Long-range transport of dust to the Baltic Sea region. *Int. J. Environ. Pollut.* 22, 72–86. https://doi.org/10.1504/IJEP.2004.005493

Huang, J., Ji, M., Xie, Y., Wang, S., He, Y., Ran, J., (2016). Global semi-arid climate change over last 60 years. *Clim. Dyn.* 46, 1131–1150. https://doi.org/10.1007/s00382-015-2636-8

Huang, J., Li, Y., Fu, C., Chen, F., Fu, Q., Dai, A., Shinoda, M., Ma, Z., Guo, W., Li, Z., Zhang, L., Liu, Y., Yu, H., He, Y., Xie, Y., Guan, X., Ji, M., Lin, L., Wang, S., Wang, G., (2017). Dryland Climate Change: Recent Progress and Challenges: Dryland Climate Change. *Rev. Geophys.* 55. https://doi.org/10.1002/2016RG000550

Hussein, T., Li, X., Al-Dulaimi, Q., Daour, S., Atashi, N., Viana, M., Alastuey, A., Sogacheva, L., Arar, S., Al-Hunaiti, A., Petäjä, T., (2020). Particulate Matter Concentrations in a Middle Eastern City – An Insight to Sand and Dust Storm Episodes. *Aerosol Air Qual. Res.* 20, 2780–2792. https://doi.org/10.4209/aaqr.2020.05.0195

Indoitu, R., Orlovsky, L., Orlovsky, N., (2012). Dust storms in Central Asia: Spatial and temporal variations. *J. Arid Environ.* 85, 62–70. https://doi.org/10.1016/j.jaridenv.2012.03.018

Issanova, G., Abuduwaili, J., (2017). Aeolian processes as dust storms in the deserts of Central Asia.

https://doi.org/10.1007/978-981-10-3190-8

Issanova, G., Abuduwaili, J., Kaldybayev, A., Semenov, O., Dedova, T., 2015. Dust storms in Kazakhstan: Frequency and division. *J. Geol. Soc. India* 85, 348–358. https://doi.org/10.1007/s12594-015-0224-5

Jickells, T.D., An, Z.S., Andersen, K.K., Baker, A.R., Bergametti, G., Brooks, N., Cao, J.J., Boyd, P.W., Duce, R.A., Hunter, K.A., Kawahata, H., Kubilay, N., laRoche, J., Liss, P.S., Mahowald, N., Prospero, J.M., Ridgwell, A.J., Tegen, I., Torres, R., (2005). Global Iron Connections Between Desert Dust, *Ocean Biogeochemistry, and Climate. Science* (80-.). 308, 67 LP – 71. https://doi.org/10.1126/science.1105959

Kang, J.H., Keller, J.J., Chen, C.S., Lin, H.C., (2012). Asian Dust Storm Events are Associated With an Acute Increase in Pneumonia Hospitalization. *Ann. Epidemiol.* 22, 257–263. https://doi.org/10.1016/j.annepidem.2012.02.008

Karaca, F., Anil, I., Alagha, O., (2009). Long-range potential source contributions of episodic aerosol events to PM10 profile of a megacity. *Atmos. Environ.* 43, 5713–5722. https://doi.org/10.1016/j.atmosenv.2009.08.005

Kashima, S., Yorifuji, T., Bae, S., Honda, Y., Lim, Y.H., Hong, Y.C., (2016). Asian dust effect on cause-specific mortality in five cities across South Korea and Japan. *Atmos. Environ.* 128, 20–27. https://doi.org/10.1016/j.atmosenv.2015.12.063

Kaskaoutis, D., Rashki, A., Houssos, E., Legrand, M., Francois, P., Bartzokas, A., Kambezidis, H., Dumka, D.U., Goto, D., Takemura, T., (2017). Assessment of changes in atmospheric dynamics and dust activity over southwest Asia using the Caspian Sea–Hindu Kush Index. *Int. J. Climatol.* 37. https://doi.org/10.1002/joc.5053

Kaskaoutis, D.G., Francis, D., Rashki, A., Chaboureau, J.P., Dumka, U.C., (2019). Atmospheric Dynamics from Synoptic to Local Scale During an Intense Frontal Dust Storm over the Sistan Basin in Winter 2019. *Geosci.* . https://doi.org/10.3390/geosciences9100453

Kaskaoutis, D.G., Houssos, E.E., Rashki, A., Francois, P., Legrand, M., Goto, D., Bartzokas, A., Kambezidis, H.D., Takemura, T., (2016). The Caspian Sea–Hindu Kush Index (CasHKI): A regulatory factor for dust activity over southwest Asia. *Glob. Planet. Change* 137, 10–23. https://doi.org/10.1016/j.gloplacha.2015.12.011

Kismelyeva, S., Khalikhan, R., Torezhan, A., Kumisbek, A., Akimzhanova, Z., Karaca, F., Guney, M., (2021). Potential Human Exposure to Mercury (Hg) in a Chlor-Alkali Plant Impacted Zone: Risk Characterization Using Updated Site Assessment Data. *Sustain.* . https://doi.org/10.3390/su132413816

Kok, J.F., Ridley, D.A., Zhou, Q., Miller, R.L., Zhao, C., Heald, C.L., Ward, D.S., Albani, S., Haustein, K., (2017). Smaller desert dust cooling effect estimated from analysis of dust size and abundance. *Nat. Geosci.* 10, 274–278. https://doi.org/10.1038/ngeo2912

Kok, J.F., Ward, D.S., Mahowald, N.M., Evan, A.T., (2018). Global and regional importance of the direct dust-climate feedback. *Nat. Commun.* 9, 241. https://doi.org/10.1038/s41467-017-02620-y

Lau, A., Shafiee, M., Smoot, G., Grossan, B., Li, S., & Maksut, Z. (2020). On-sky SiPM Performance Measurements for Millisecond to Sub-Microsecond Optical Source Variability Studies.

Laurent, B., Marticorena, B., Bergametti, G., Mei, F., (2006). Modeling mineral dust emissions from

Chinese and Mongolian deserts. *Glob. Planet. Change* 52, 121–141. https://doi.org/10.1016/j.gloplacha.2006.02.012

Li, Y., Song, Y., Kaskaoutis, D., Zan, J., Orozbaev, R., Tan, L., (2021). Aeolian dust dynamics in the Fergana Valley, Central Asia, since ~30 ka inferred from loess deposits. *Geosci. Front.* https://doi.org/10.1016/j.gsf.2021.101180.

Li, Y., Song, Y., Kaskaoutis, D.G., Chen, X., Mamadjanov, Y., Tan, L., (2019). Atmospheric dust dynamics in southern Central Asia: implications for buildup of Tajikistan loess sediments. *Atmos. Res.* 229, 74–85.

Li, Y., Song, Y., Kaskaoutis, D.G., Zhang, X., Chen, X., Shukurov, N., Orozbaev, R., (2022). Atmospheric dust dynamics over Central Asia: A perspective view from loess deposits. *Godwana Research* 109, 150-165, https://doi.org/10.1016/j.gr.2022.04.019.

Liakakou, E., Stavroulas, I., Kaskaoutis, D.G., Grivas, G., Paraskevopoulou, D., Dumka, U.C., Tsagkaraki, M., Bougiatioti, A., Oikonomou, K., Sciare, J., Gerasopoulos, E., Mihalopoulos, N., 2020. Long-term variability, source apportionment and spectral properties of black carbon at an urban background site in Athens, Greece. *Atmos. Environ.* 222, 117137.

Madruga, D.G., Ubeda, R.M., Terroba, J.M., Dos Santos, S.G., García-Cambero, J.P., (2019). Particle-associated polycyclic aromatic hydrocarbons in a representative urban location (indoor-outdoor) from South Europe: Assessment of potential sources and cancer risk to humans. *Indoor Air* 29, 817–827. https://doi.org/10.1111/ina.12581

Maghrabi, A., Alharbi, B., Tapper, N., (2011). Impact of the March 2009 dust event in Saudi Arabia on aerosol optical properties, meteorological parameters, sky temperature and emissivity. *Atmos. Environ.* 45, 2164–2173. https://doi.org/10.1016/J.ATMOSENV.2011.01.071

Mahmoodirad, A., Dehghan, R., Niroomand, S., (2019). Modelling linear fractional transportation problem in belief degree-based uncertain environment, *J Exp Theor Artif Intell,* 31,3, 393-408.

Mahmoodirad, A., Sanei, M., (2016). Solving a multi-stage multi-product solid supply chain network design problem by meta-heuristics, *Scientia Iranica,* 23, 3, 1429-1440.

Mahowald, N., Albani, S., Kok, J.F., Engelstaeder, S., Scanza, R., Ward, D.S., Flanner, M.G., (2014). The size distribution of desert dust aerosols and its impact on the Earth system. *Aeolian Res.* 15, 53–71. https://doi.org/10.1016/j.aeolia.2013.09.002

Martínez, M.A., Ruiz, J., Cuevas, E., (2009). Use of SEVIRI images and derived products in a WMO Sand and dust Storm Warning System. IOP Conf. *Ser. Earth Environ. Sci.* 7, 12004. https://doi.org/10.1088/1755-1307/7/1/012004

Middleton, N., (2017). Desert dust hazards: A global review. *Aeolian Res.*, 24, 53-63.

Middleton, N., (2020). Health in dust belt cities and beyond—an essay by Nick Middleton. *BMJ* 371, m3089. https://doi.org/10.1136/bmj.m3089

Middleton, N., Kang, U., (2017). Sand and Dust Storms: Impact Mitigation. *Sustainability* 9, 1053. https://doi.org/10.3390/su9061053

Middleton, N., Kashani, S.S., Attarchi, S., Rahnama, M., Mosalman, S.T., (2021). Synoptic Causes and Socio-Economic Consequences of a Severe Dust Storm in the Middle East. *Atmosphere* (Basel).

12. https://doi.org/10.3390/atmos12111435

Miller, R., Cakmur, R., Perlwitz, J., Geogdzhayev, I., Ginoux, P., Koch, D., Kohfeld, K., Prigent, C., Ruedy, R., Schmidt, G., Tegen, I., (2006). Mineral dust aerosols in the NASA Goddard Institute for Space Sciences ModelE atmosphere general circulation model. *J. Geophys. Res.* 111. https://doi.org/10.1029/2005JD005796

MKWEATHER, (2021). Uzbekistan and southern Kazakhstan hit the worst dust storm in recorded history.

Mohammadpour, K., Sciortino, M., Kaskaoutis, D., Rashki, A., (2022). Classification of synoptic weather clusters associated with dust accumulation over southeastern areas of the Caspian Sea (Northeast Iran and Karakum desert). *Aeolian Res.* 54. https://doi.org/10.1016/j.aeolia.2022.100771

Molla-Alizadeh-Zavardehi, S., Mahmoodirad, A., Rahimian, M., (2014). Step Fixed Charge Transportation Problems via Genetic Algorithm, *Indian J. Sci. Technol.*, 7,7, 949-954.

Niroomand, S., Harish Garg, H., Ali Mahmoodirad, A., (2020). An intuitionistic fuzzy two stage supply chain network design problem with multi-mode demand and multi-mode transportation, *ISA Transactions*, 107, 117-133.

Nobakht, M., Shahgedanova, M., White, K., (2021). New Inventory of Dust Emission Sources in Central Asia and Northwestern China Derived From MODIS Imagery Using Dust Enhancement Technique. *J. Geophys. Res. Atmos.* 126, e2020JD033382. https://doi.org/10.1029/2020JD033382

NPRK, (2005). National Program for struggle against land desertification in the Republic of Kazakhstan for 2005–2015 years,Government Resolution # 49.

Perez, L., Tobias, A., Querol, X., Künzli, N., Pey, J., Alastuey, A., Viana, M., Valero, N., Gonz&xe1;lez-Cabré, M., Sunyer, J., (2008). Coarse Particles From Saharan Dust and Daily Mortality. *Epidemiology* 19, 800–807.

Prakash, P., Stenchikov, G., Kalenderski, S., Osipov, S., Bangalath, H.K., (2015). The impact of dust storms on the Arabian Peninsula and the Red Sea. *Atmos. Chem. Phys.* 15, 199–222. https://doi.org/10.5194/acp-15-199-2015

Ramazanova, E., Lee, S.H., Lee, W., (2021). Stochastic risk assessment of urban soils contaminated by heavy metals in Kazakhstan. *Sci. Total Environ.* 750, 141535. https://doi.org/10.1016/j.scitotenv.2020.141535

Rashki, A., Kaskaoutis, D.G., Francois, P., Kosmopoulos, P.G., Legrand, M., (2015). Dust-storm dynamics over Sistan region, Iran: Seasonality, transport characteristics and affected areas. *Aeolian Res.* 16, 35–48. https://doi.org/10.1016/J.AEOLIA.2014.10.003

Rupakheti, D., Rupakheti, M., Yin, X.F., Hofer, J., Rai, M., Hu, Y.L., Abdullaev, S.F., Kang, S.C., (2021). Modifications in aerosol physical, optical and radiative properties during heavy aerosol events over Dushanbe, Central Asia. *Geosci. Front.*, 12, 101251.

Rupakheti, D., Kang, S., Bilal, M., Gong, J., Xia, X., Cong, Z., (2019). Aerosol optical depth climatology over Central Asian countries based on Aqua-MODIS Collection 6.1 data: aerosol variations and sources. *Atmos. Environ*. 207, 205–214. https://doi.org/ 10.1016/j.atmosenv.2019.03.020.

Rupakheti, D., Rupakheti, M., Abdullaev, S.F., Yin, X., Kang, S., (2020). Columnar aerosol properties and radiative effects over Dushanbe, Tajikistan in Central Asia. *Environ. Pollut*. 265, 114872.

Sayer, A.M., Hsu, N.C., Lee, J., Kim, W., Dutcher, S.T., (2019). Validation, Stability, and Consistency of MODIS Collection 6.1 and VIIRS Version 1 Deep Blue Aerosol Data Over Land. *J. Geophys. Res. Atmos.*

Schepanski, K., (2018). Transport of Mineral Dust and Its Impact on Climate. Geosciences 2018, 8, 151; doi:10.3390/geosciences8050151.

Schepanski, K., Tegen, I., Laurent, B., Heinold, B., Macke, A.A., (2007). new Saharan dust source activation frequency map derived from MSG-SEVIRI IR-channels. *Geophys. Res. Lett.* 34, L18803.

Schepanski, K., Tegen, I., Macke, A., (2009). Saharan dust transport and deposition towards the tropical northern Atlantic. *Atmos. Chem. Phys.* 9, 1173–1189.

Shafiee, M., Fedorov, D., Grossan, B., Kizheppatt, V., & Smoot, G. (2021). A readout system for microwave kinetic inductance detectors using software defined radios. *J. Instrument.*, 16, P07015. https://doi.org/10.1088/1748-0221/16/07/P07015

Shafiee, M., Feghhi, S. A. H., & Rahighi, J. (2017). Experimental performance evaluation of ILSF BPM data acquisition system. *Measurement*, 100, 205–212. https://doi.org/10.1016/j.measurement.2017.01.003

Shafiee, M., Grossan, B., Hu, J., Colantoni, I., & Smoot, G. (2019). Design optimization of a 10 kilopixel optical band Microwave Kinetic Inductance Detector. *J. Instrument.*, 14(12), P12011--P12011. https://doi.org/10.1088/1748-0221/14/12/p12011

Shaheen, A., Wu, R., Aldabash, M., (2020). Long-term AOD trend assessment over the Eastern Mediterranean region: A comparative study including a new merged aerosol product. *Atmos. Environ.* 238, 117736.

Shi, L., Zhang, J.H., Yao, F., Zhang, D., Guo, H., (2019). Temporal variation of dust emissions in dust sources over Central Asia in recent decades and the climate linkages. *Atmos. Environ.* 222, 117176. https://doi.org/10.1016/j.atmosenv.2019.117176

Solomos, S., Kalivitis, N., Mihalopoulos, N., Amiridis, V., Kouvarakis, G., Gkikas, A., Binietoglou, I., Tsekeri, A., Kazadzis, S., Kottas, M., Pradhan, Y., Proestakis, E., Nastos, P.T., Marenco, F., (2018). From tropospheric folding to Khamsin and foehn winds: how atmospheric dynamics advanced a record-breaking dust episode in Crete. *Atmosphere* 9, 240. https://doi.org/10.3390/atmos9070240.

Song, Y., Li, Y., Cheng, L., Zong, X., Kang, S., Ghafarpour, A., Li, X., Sun, H., Fu, X., Dong, J., Mamadjanov, Y., Orozbaev, R., Shukurov, N., Gholami, H., Shukurov, S., Xie, M., (2021). Spatio-temporal distribution of Quaternary loess across Central Asia. *Palaeogeogr. Palaeoclimatol. Palaeoecol.* 567, 110279. https://doi.org/10.1016/j.palaeo.2021.110279

Sternberg, T., Edwards, M., (2017). Desert Dust and Health: A Central Asian Review and Steppe Case Study. *Int. J. Environ. Res. Public Health* 14, 1342. https://doi.org/10.3390/ijerph14111342

Tegen, I., Lacis, A., (1996). Modeling of particle size distribution and its influence on the radiative properties of mineral dust aerosol. *J. Geophys. Res.* 1011, 19237–19244. https://doi.org/10.1029/95JD03610

Tositti, L., Brattich, E., Cassardo, C., Morozzi, P., Bracci, A., Marinoni, A., Di Sabatino, S., Porcù, F., Zappi, A., (2022). Development and evolution of an anomalous Asian dust event across Europe in March 2020. *Atmos. Chem. Phys.*, 22, 4047–4073, https://doi.org/10.5194/acp-22-4047-2022.

UN, (2010). UN Shrinking Aral Sea Underscores Need for Urgent Action on Environment.

Uno, I., Eguchi, K., Yumimoto, K., Takemura, T., Shimizu, A., Uematsu, M., Liu, Z., Wang, Z., Hara, Y., Sugimoto, N., (2009). Asian dust transported one full circuit around the globe. *Nat. Geosci.* 2. https://doi.org/10.1038/NGEO583

Uzhydromet, (2021). Available at https://hydromet.uz/

Wang, C.H., Chen, C.S., Lin, C.L., (2014). The threat of Asian dust storms on asthma patients: a population-based study in Taiwan. *Glob. Public Health* 9, 1040–1052. https://doi.org/10.1080/17441692.2014.951871

Wang, F., Zhao, X., Gerlein-Safdi, C., Mu, Y., Wang, D., Lu, Q., (2017). Global sources, emissions, transport and deposition of dust and sand and their effects on the climate and environment: a review. *Front. Environ. Sci. Eng.* 11, 13. https://doi.org/10.1007/s11783-017-0904-z

WHO, (2021). WHO Air quality guidelines for particulate matter, ozone, nitrogen dioxide and sulfur dioxide.

Wiggs, G., O'Hara, S., Wegerdt, J., Van Der Meer, J., Small, I., Hubbard, R., (2003). The dynamics and characteristics of aeolian dust in dryland Central Asia: Possible impacts on human exposure and respiratory health in the Aral Sea basin. *Geogr. J.* 169. https://doi.org/10.1111/1475-4959.04976

Wu, Y., Wen, B., Li, S., Guo, Y., (2021). Sand and dust storms in Asia: a call for global cooperation on climate change. *Lancet Planet. Heal*. 2021. https://doi.org/10.1016/S2542-5196(21)00082-6

Xi, X., Sokolik, I.N., (2015). Dust interannual variability and trend in Central Asia from 2000 to 2014 and their climatic linkages. *J. Geophys. Res. Atmos.* 120, 12,112-175,197. https://doi.org/10.1002/2015JD024092

Zhang, X.X., Claiborn, C., Lei, J.Q., Vaughan, J., Wu, S.X., Li, S.Y., Liu, L.Y., Wang, Z.F., Wang, Y.D., Huang, S.Y., Zhou, J., (2020). Aeolian dust in Central Asia: Spatial distribution and temporal variability. *Atmos. Environ.* 238, 117734. https://doi.org/10.1016/j.atmosenv.2020.117734

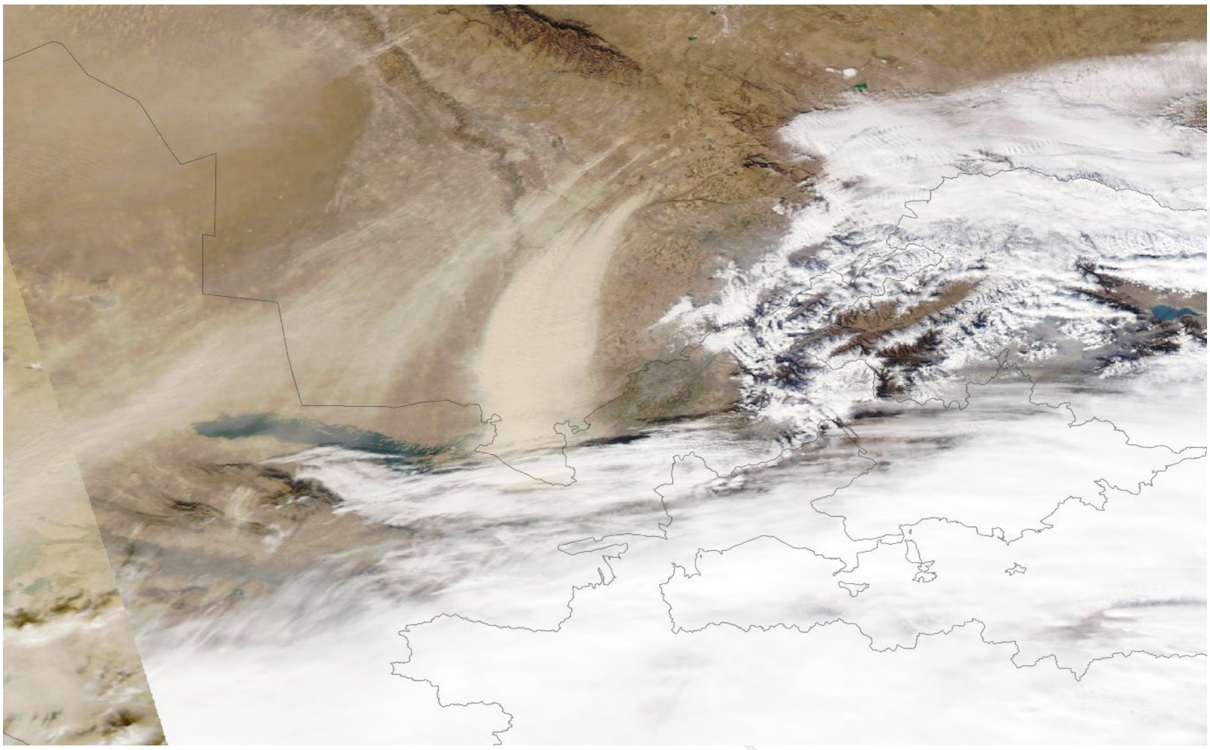

Figure 1: True colour image from the Terra-MODIS sensor (https://worldview.earthdata.nasa.gov) on 4th November 2021, focused on the dust storm.

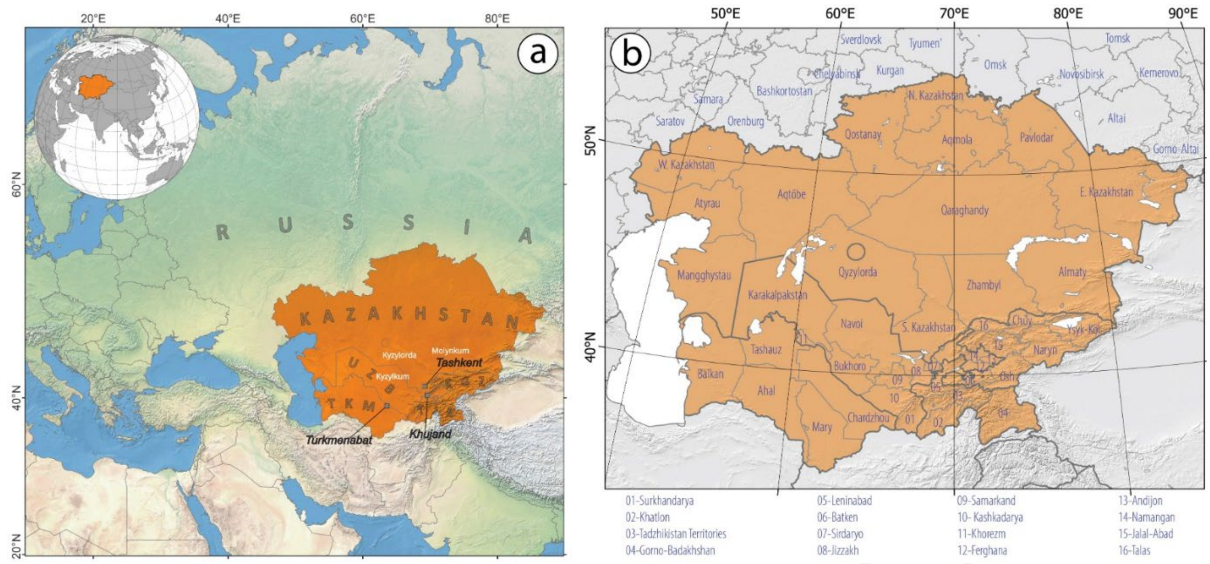

Figure 2: Physiographic map of the study area highlighting the Central Asian countries.

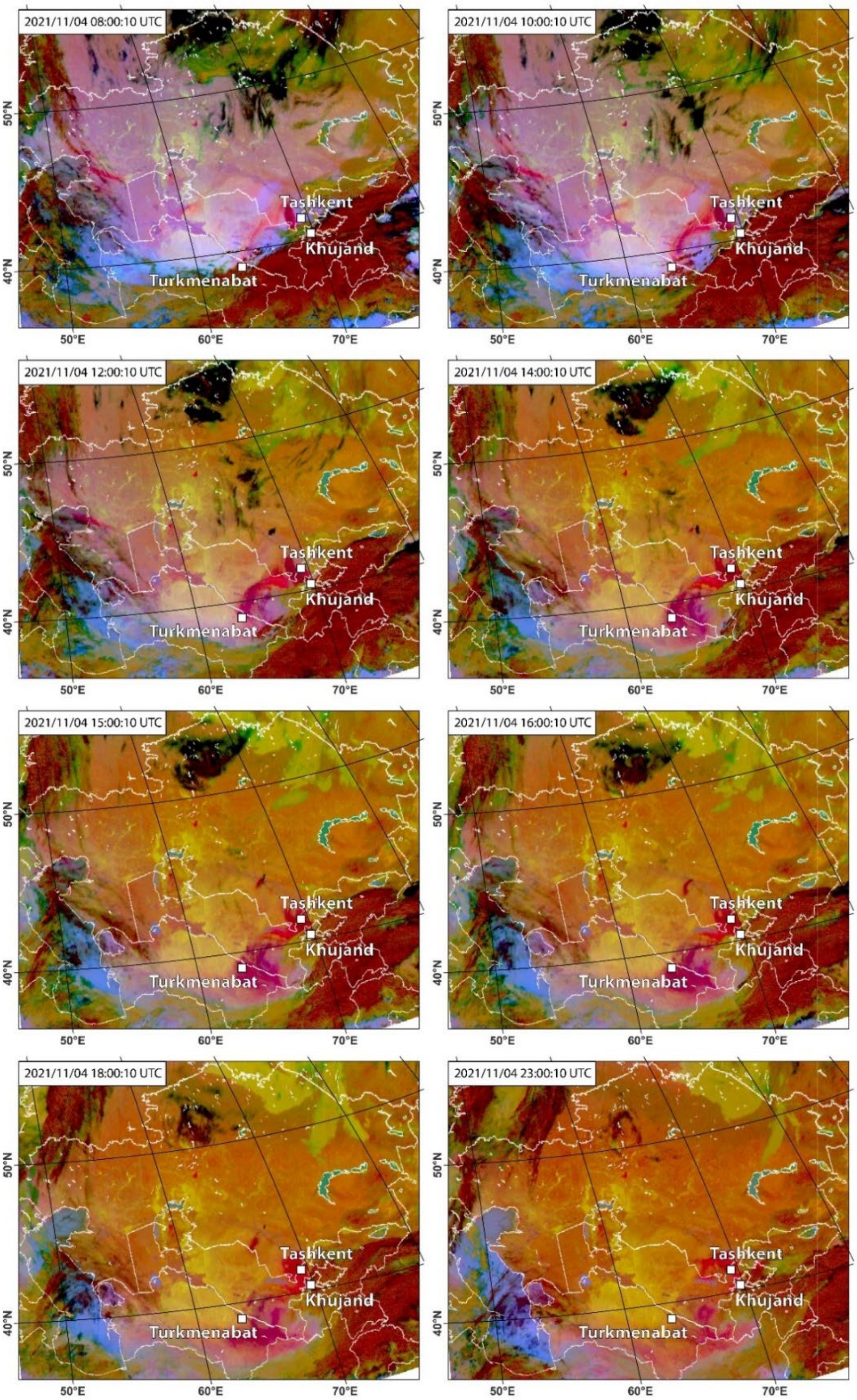

Figure 3: SEVIRI satellite images over Central Asia at different hours on 4 November 2021, detecting the evolution of the thick dust plume (in pink/magenta). The key receptor sites of Tashkent in Uzbekistan, Khujand in Tajikistan and Turkmenabat in Turkmenistan are also shown.

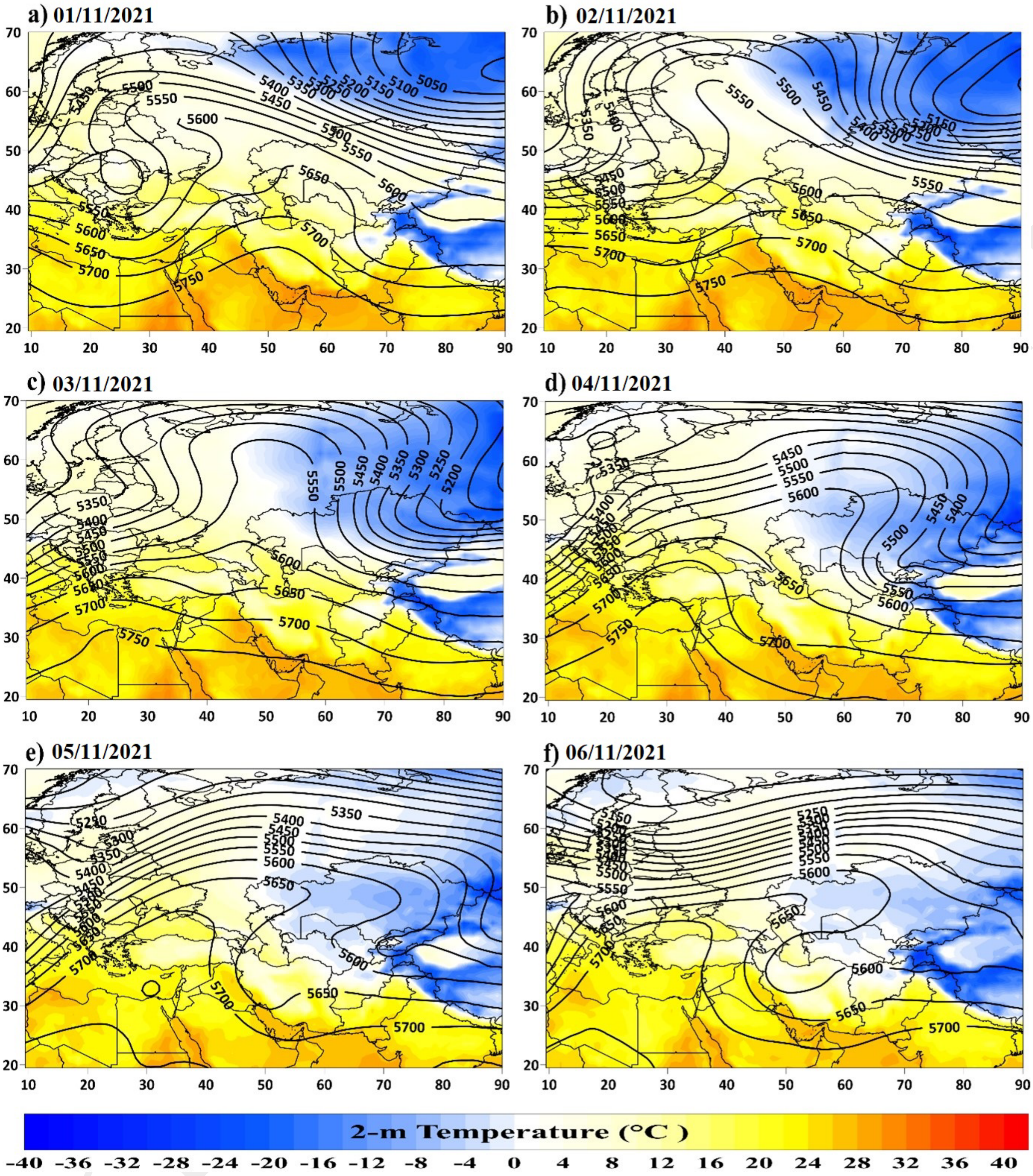

Figure 4: Composite maps of geopotential heights at 500 hPa (black contours) and surface temperature (shaded area) from 1 to 6 November 2021 (a - f).

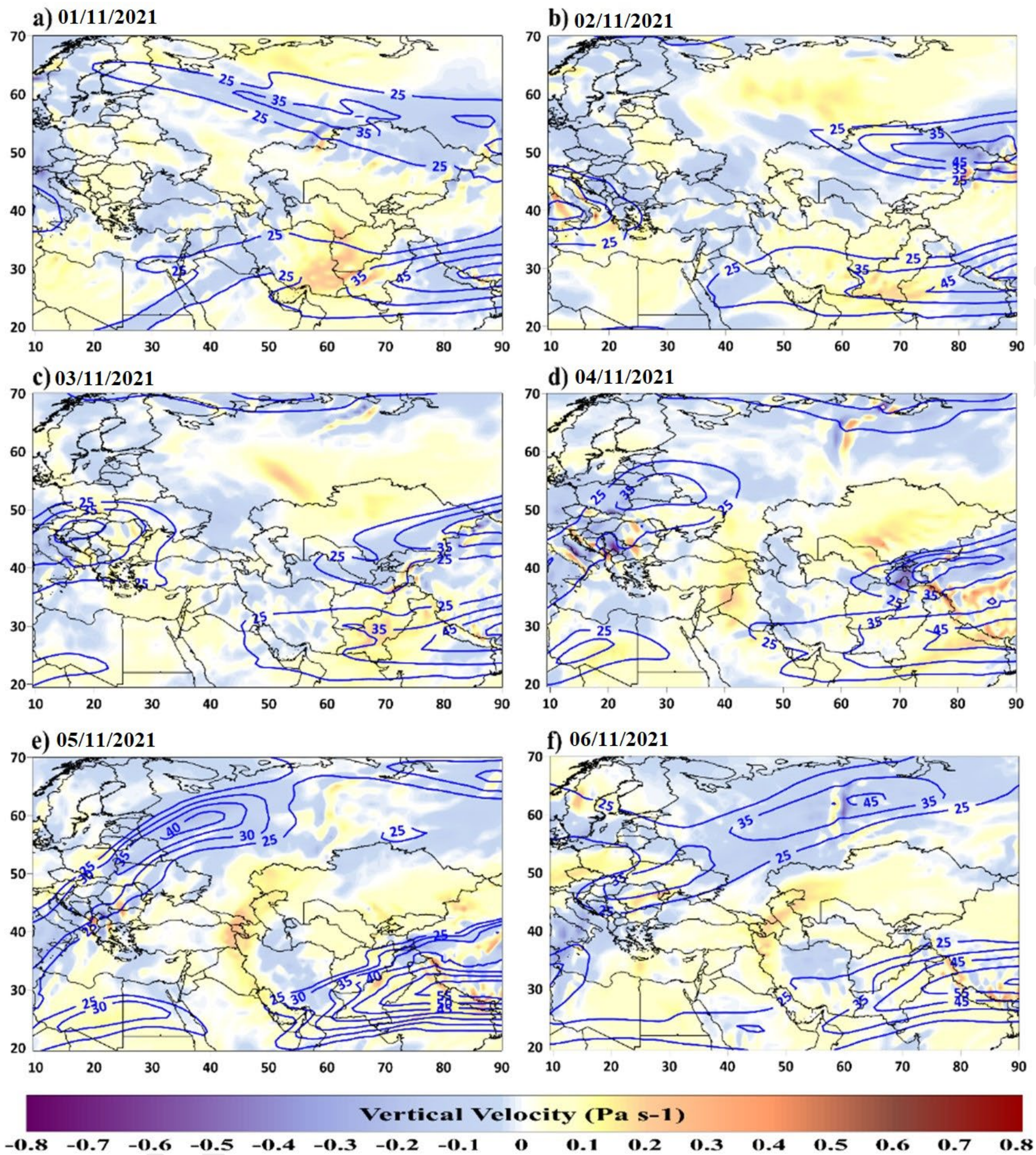

Figure 5: Composite maps of omega at 300 hPa (shaded area) and zonal wind at 250 hPa (blue contours) from 1 to 6 November 2021 (a - f).

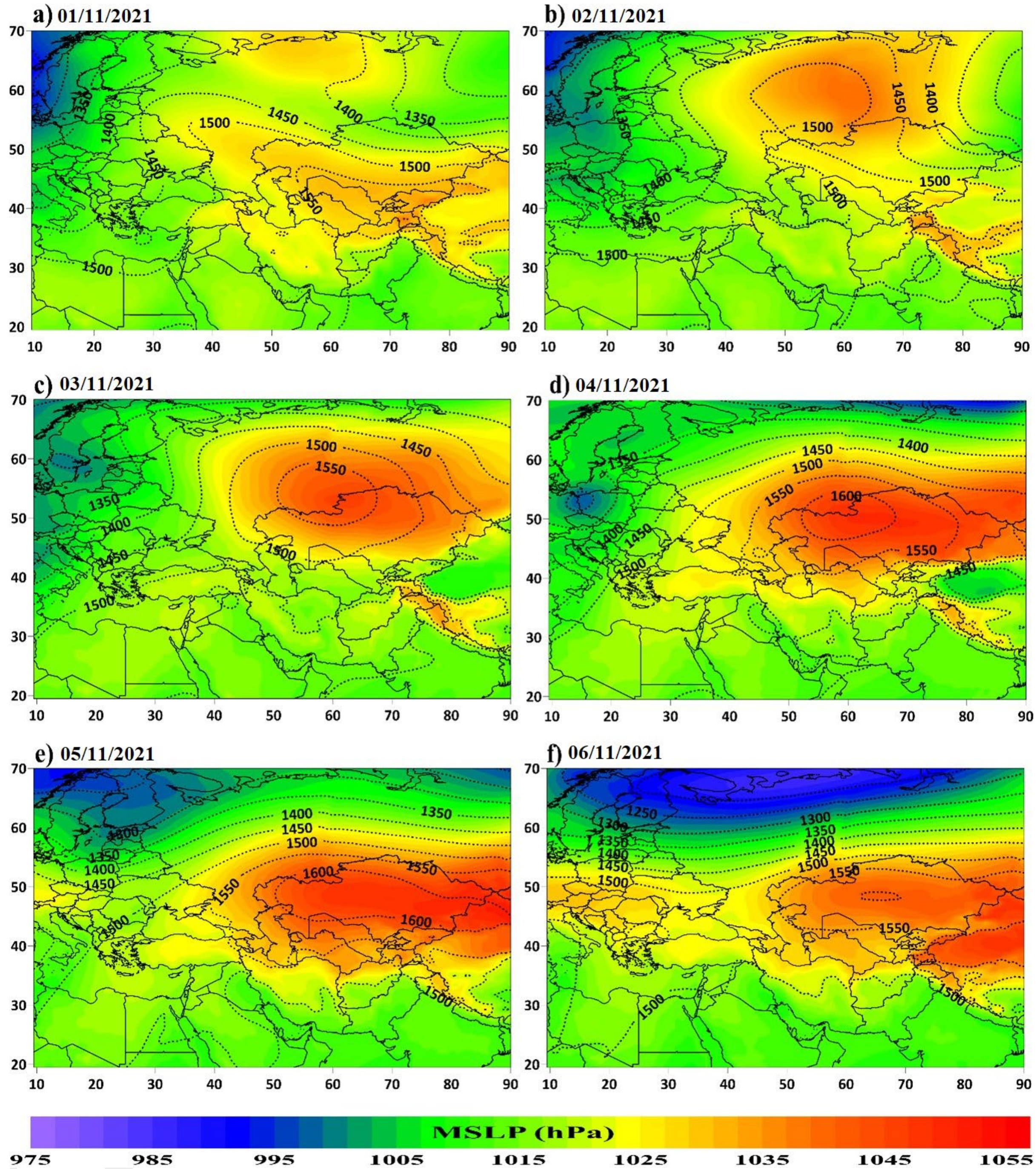

Figure 6: Composite maps of geopotential heights at 850 hPa (dash black contours) and mean sea-level pressure (MSLP, shaded area) from 1st to 6th November 2021 (a - f).

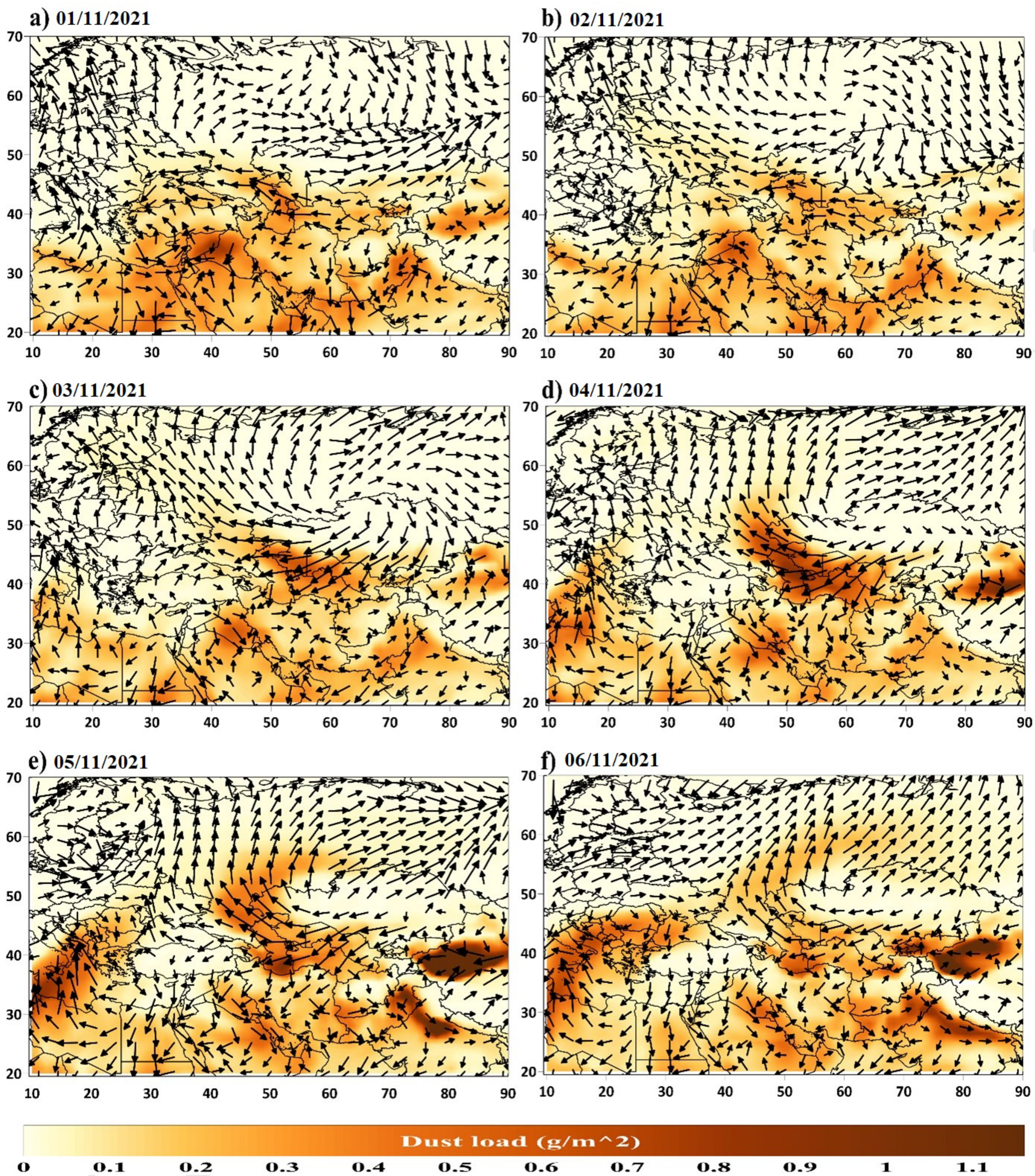

Figure 7: Composite maps of dust load (g m^{-2}) and surface vector winds (m s^{-1}) from 1st to 6th November 2021 (a-f).

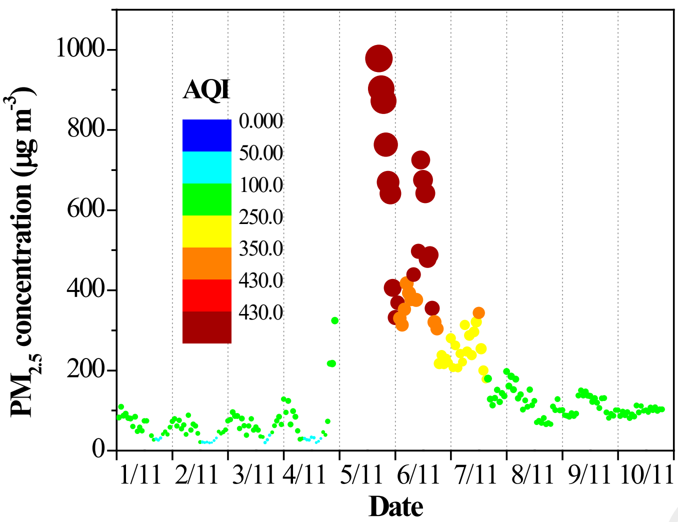

Figure 8: Hourly $PM_{2.5}$ concentrations in Tashkent around the dust storm day (4th November 2021), color-coded with the AQI values.

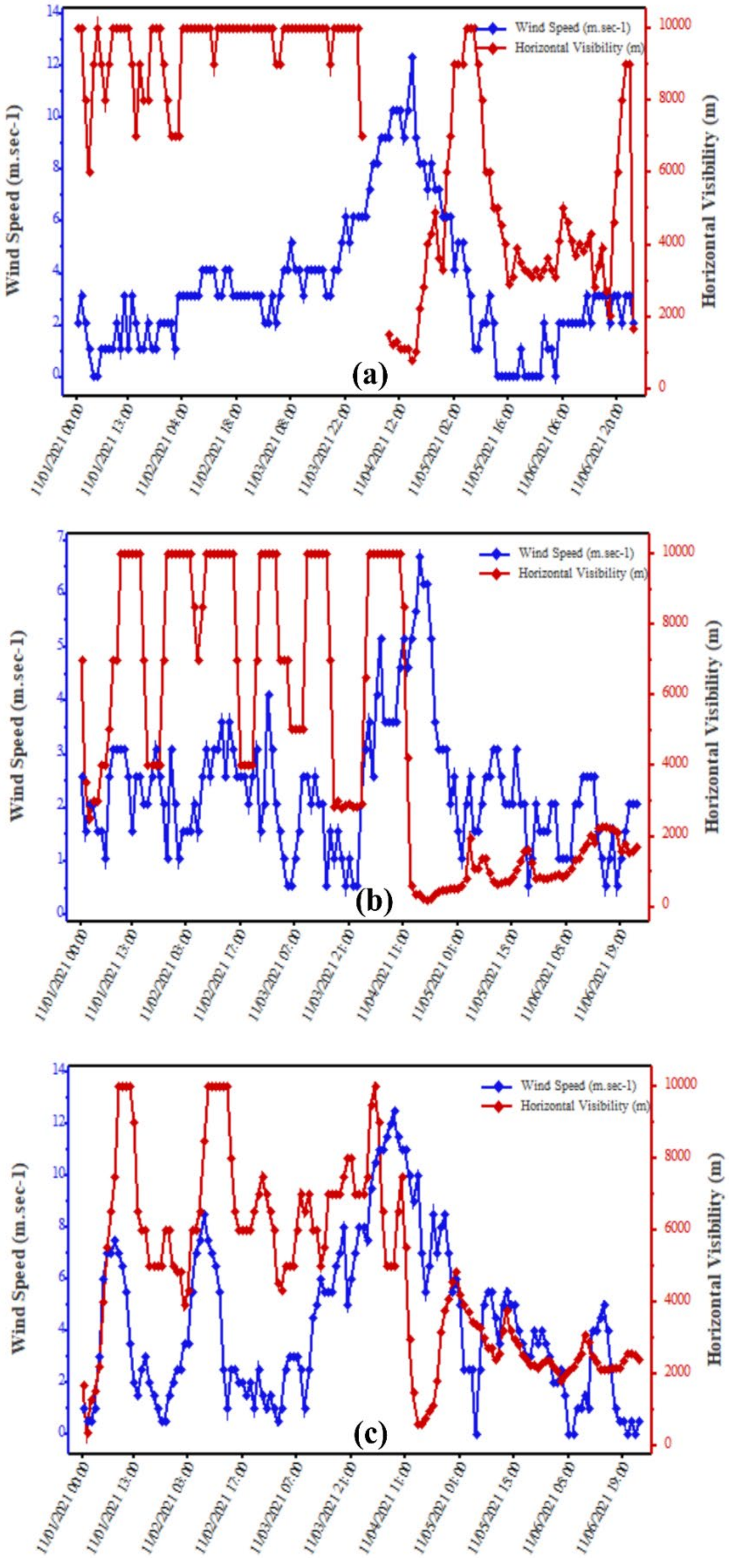

Figure 9: Hourly ground-based measurements of wind speed and horizontal visibility at stations in Central Asia, (a) Turkmenabat, (b) Tashkent and (c) Khujand during 1-6 November 2021.

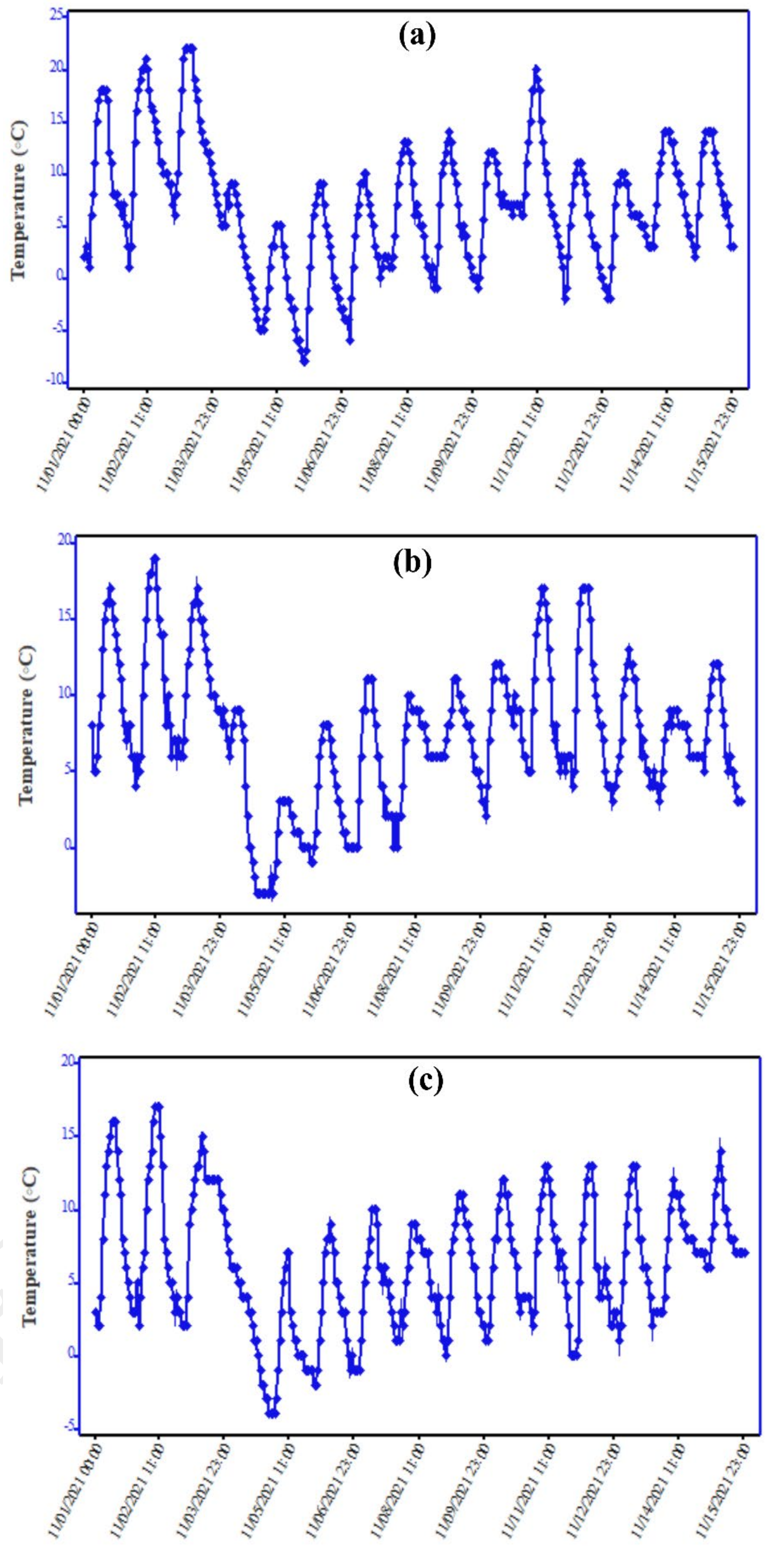

Figure 10: The hourly ground-based measurements (2-m temperature) for the study stations of (a) Turkmenabat (b) Tashkent, and (c) Khujand between 1-15 November 2021.

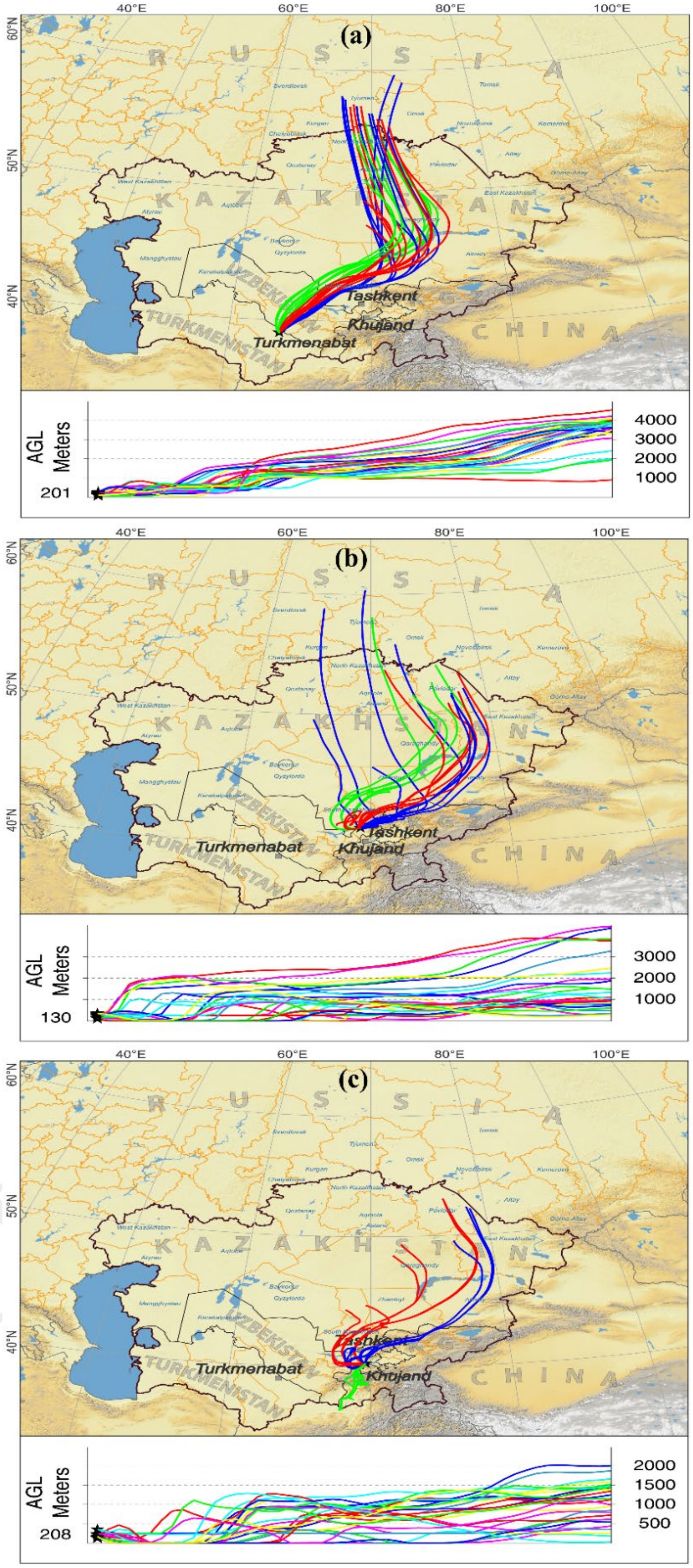

Figure 11: Backward trajectory analysis by HYSPLIT model at receptor sites of (a) Turkmenabat, (b) Tashkent and (c) Khujand on 4th November 2021 (the dust storm day).